RICE UNIVERSITY

New approaches for incorporating the exact exchange energy density into density functional approximations

by

Aliaksandr Krukau

A Thesis Submitted
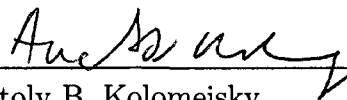in Partial Fulfillment of the
Requirements for the Degree

Doctor of Philosophy

Approved, Thesis Committee:

Gustavo E. Scuseria, Chairman
Robert A. Welch Professor of Chemistry

Anatoly B. Kolomeisky
Associate Professor of Chemistry

Qimiao Si
Harry C. and Olga K. Wiess Professor of
Physics and Astronomy

Houston, Texas

April, 2009

UMI Number: 3362345

INFORMATION TO USERS

The quality of this reproduction is dependent upon the quality of the copy submitted. Broken or indistinct print, colored or poor quality illustrations and photographs, print bleed-through, substandard margins, and improper alignment can adversely affect reproduction.
In the unlikely event that the author did not send a complete manuscript and there are missing pages, these will be noted. Also, if unauthorized copyright material had to be removed, a note will indicate the deletion.

UMI®

Abstract

New approaches for incorporating the exact exchange energy density into density functional approximations

by

Aliaksandr Krukau

In the last ten years, hybrid density functional approximations have become the most widely used method in modern quantum chemistry. Hybrid functionals combine the semi-local exchange-correlation and a fraction of the exact-exchange energy. The most common are global hybrid functionals, with a constant fraction of the exact exchange determined emprirically. Recently, two complementary strategies have been proposed to improve the performance of hybrid functionals. In range-separated hybrid functionals, the fraction of exact exchange depends on the interelectronic distance. In local hybrid functionals, the fraction of exact exchange is position-dependent. In this work, we propose two approaches that combine range-separated and local hybrid functionals together, providing a promising route to more accurate results.

Most previous implementations of range-separated hybrid functionals use a universal, system-independent screening parameter, fitted to experimental data. However, the screening parameter proves to depend strongly on the choice of the training

set. Moreover, such functionals violate the exact high-density limit. In this work, we argue that the separation between short-range (SR) and long-range (LR) interactions should depend on the local density. We propose an approximation that uses a position-dependent screening function $\omega(\mathbf{r})$ defining a *local* range separation (LRS) for mixing exact (HF-type) and LSDA exchange. This method adds a substantial flexibility to describe diverse chemical compounds. Moreover, the new model satisfies a high-density limit better than the approximation with fixed screening parameter.

We have also developed an alternative strategy to improve the range-separated functionals by combining them together with local hybrid functionals. We consider two limiting cases: screened local hybrids with short-range exact exchange, and long-range corrected hybrids with long-range exact exchange. The former approach can treat metals and narrow-gap semiconductors much more efficiently than standard local hybrids do. The latter method provides the correct asymptotic behavior, which is important for the treatment of charge transfer and Rydberg excitations in finite systems.

Acknowledgments

I would like to thank my advisor Prof. Gustavo Scuseria for allowing me to join his oustanding research group. Prof. Scuseria is a wonderful mentor and a great person, and I am proud that I worked in his laboratory. I am indebted to my collaborators: Prof. John Perdew, Prof. Andreas Savin, Prof. Viktor Staroverov, Dr. Benjamin Janesko, Dr. Oleg Vydrov, and Dr. Jochen Heyd who shared their extraordinary ideas with me. I want to thank Dr. Thomas Henderson, Dr. Cristian Diaconu, and all other members of Scuseria's group for enlightening discussions. And, of course, I appreciate the constant support from my parents.

Contents

Illustrations

Tables

Preface

This thesis is based on my research conducted at Rice University. Most of the results presented here have been previously published in the following papers:

- Aliaksandr V. Krukau, Gustavo E. Scuseria, John P. Perdew,
  and Andreas Savin,
  Hybrid functionals with local range separation
  J. Chem. Phys. **129**, 124103 (2008).

- Benjamin G. Janesko, Aliaksandr V. Krukau, and Gustavo E. Scuseria,
  Self-consistent generalized Kohn-Sham local hybrid functionals of screened exchange: Combining local and range-separated hybridization
  J. Chem. Phys. **129**, 124110 (2008).

Dr. Benjamin Janesko implemented and tested the self-consistent version of the code for range-separated local hybrids described in chapter 4. I prepared and tested the initial, non-self-consistent version of the code.

Abbreviations

AO   —   atomic orbital

c   —   correlation

DFT   —   density functional theory

DFA   —   density functional approximation

FR   —   full-range

GKS   —   generalized Kohn-Sham

GGA   —   generalized gradient approximation

HF   —   Hartree–Fock (or Hartree–Fock–like)

HSE   —   Heyd–Scuseria–Ernzerhof

KS   —   Kohn–Sham

Lh   —   local hybrid

LC   —   long-range corrected

LR   —   long range

LSDA   —   local spin density approximation

ME   —   mean error

MAE   —   mean absolute error

PBE   —   Perdew–Burke–Ernzerhof

RI   —   resolution of the identity

SC   —   screened

SCF   —   self-consistent field

SR   —   short range

TPSS   —   Tao–Perdew–Staroverov–Scuseria

x   —   exchange

xc   —   exchange-correlation

Chapter 1

Introduction to density functional theory

1.1 Kohn–Sham formalism

In the last twenty years, density functional theory (DFT) has become one of the most popular methods in modern quantum chemistry and solid state physics. DFT often provides highly accurate description of electronic structure with computational cost that is substantially lower than the cost of many-particle methods. The foundation of DFT is based on the first Hohenberg-Kohn theorem [1]. It states that the ground-state energy of a many-electron system is a unique functional of the ground-state electronic density $\rho(\mathbf{r}_1)$, where the density is defined as:

$$\rho(\mathbf{r}_1) = N \sum_{\sigma_1...\sigma_N} \int ... \int |\Psi(\mathbf{r}_1, \sigma_1, \mathbf{r}_2, \sigma_2, ..., \mathbf{r}_N, \sigma_N)|^2 d\mathbf{r}_2...d\mathbf{r}_N. \tag{1.1}$$

Practical DFT calculations are usually performed within the Kohn-Sham (KS) formalism [2]. In KS-DFT, the total energy of the electronic system with the density $\rho(\mathbf{r})$ is written as:

$$E_{\text{tot}} = -\frac{1}{2} \sum_i \langle \phi_i | \nabla^2 | \phi_i \rangle + \int \rho(\mathbf{r}) v_{\text{ext}}(\mathbf{r}) d\mathbf{r} + J[\rho] + E_{\text{xc}}[\rho], \tag{1.2}$$

where the first sum is the kinetic energy of non-interacting electrons, $\phi_i(\mathbf{r})$ are the Kohn-Sham orbitals, $v_{\text{ext}}(\mathbf{r})$ is an external potential, $J[\rho]$ is the Coulomb interaction

of the electron density with itself,

$$J[\rho] = \frac{1}{2} \int \frac{\rho(\mathbf{r})\rho(\mathbf{r}')}{|\mathbf{r}-\mathbf{r}'|} d\mathbf{r} d\mathbf{r}', \tag{1.3}$$

and E_{xc} is an exchange-correlation functional, the only term that is not known exactly. Much efforts has been directed towards the construction of more accurate approximations to E_{xc}. In Eq. (1.2), the orbitals $\phi_i(\mathbf{r})$ are the solutions of the Kohn-Sham equations [3]:

$$\left[\frac{1}{2}\nabla^2 + v_{KS}(\rho)\right] \phi_i(\mathbf{r}) = \varepsilon_i \phi_i(\mathbf{r}), \tag{1.4}$$

$$\rho(\mathbf{r}) = \sum_i n_i |\phi_i|^2, \tag{1.5}$$

where the KS effective potential v_{KS} is defined as:

$$v_{KS}(\mathbf{r}) = v_{ext}(\mathbf{r}) + \int d\mathbf{r}' \frac{\rho(\mathbf{r}')}{|\mathbf{r}-\mathbf{r}'|} + v_{xc}(\mathbf{r}), \tag{1.6}$$

and

$$v_{xc}(\mathbf{r}) = \frac{\delta E_{xc}}{\delta \rho}. \tag{1.7}$$

In DFT, it is customary to divide exchange-correlation functional into the exchange and correlation parts:

$$E_{xc} = E_x + E_c \tag{1.8}$$

The exact expression for the exchange energy is:

$$E_x^{HF} = -\frac{1}{2} \sum_{i,j}^{occ} \int \int \frac{\varphi_i^*(\mathbf{r})\varphi_j^*(\mathbf{r}')\varphi_i(\mathbf{r}')\varphi_j(\mathbf{r})}{|\mathbf{r}-\mathbf{r}'|} d\mathbf{r} d\mathbf{r}' \tag{1.9}$$

Eq. (1.9) is similar to the definition of exchange energy in Hartree-Fock theory. However, in this equation we should use the KS, not HF, orbitals. These two sets of

orbitals are the solution of different equations, and therefore they differ. In most KS-DFT calculations, an approximate exchange functional is used instead of the exact one. This is necessary because the combination of exact exchange and approximate correlation functionals usually yields poor accuracy.

1.2 Spin-DFT

In the original KS theory, exchange-correlation functional is written in terms of the total density. However, it it extremely difficult to describe the energy of spin-polarized system in terms of the total electronic density. Spin-DFT [2], an extension of KS scheme to the case of a non-zero magnetic field, provided a solution to this problem. In spin-DFT, the exchange-correlation functional depends on both the spin-up $\rho_\alpha(\mathbf{r})$ and spin-down electron densities $\rho_\beta(\mathbf{r})$. It was shown [4] that even in the absence of magnetic field the approximate density functionals $E_{\text{xc}}[\rho_\alpha, \rho_\beta]$ are much more accurate than $E_{\text{xc}}[\rho]$ (where $\rho = \rho_\alpha + \rho_\beta$). Almost all current DFT calculations are performed with spin-DFT formalism rather than original KS-DFT approach. For the exchange functional, there is a spin-scaling formula [5] that relates $E_{\text{x}}[\rho]$ and $E_{\text{x}}[\rho_\alpha, \rho_\beta]$ to each other:

$$E_{\text{x}}[\rho_\alpha, \rho_\beta] = \frac{1}{2}E_{\text{x}}[2\rho_\alpha] + \frac{1}{2}E_{\text{x}}[2\rho_\beta]. \qquad (1.10)$$

For simplicity of notation, we will not include spin indices in most of the subsequent text. It will be tacitly assumed that Eq. (1.10) should be applied in order to obtain $E_{\text{x}}[\rho_\alpha, \rho_\beta]$ exchange functional.

1.3 Approximate exchange-correlation functionals

Perdew and co-workers [6, 7] proposed to classify the existing approximate exchange-correlation functionals into a "Jacob's ladder" of approximations. The approximations at higher rungs are (hopefully) more accurate, but have a large computational cost. The methods at lower rungs are less accurate, but more computationally efficient.

The the lowest rung is the local spin density approximation (LSDA) [2]:

$$E_{xc}^{LSDA} = \int e_{xc}^{LSDA}(\rho(\mathbf{r}))d\mathbf{r}, \tag{1.11}$$

where e_{xc}^{LSDA} is obtained from the expression for a uniform electron gas with density $\rho(\mathbf{r})$. Note that the exchange density e_{xc} at any point depends only on the local density at that point.

The next level for Jacob's ladder is the generalized gradient approximations (GGA) [8] which introduce an additional "semilocal" ingredient, the density gradient $\nabla\rho(\mathbf{r})$:

$$E_{xc}^{LSDA} = \int e_{xc}(\rho(\mathbf{r}), \nabla\rho(\mathbf{r}))d\mathbf{r}. \tag{1.12}$$

The third rung is represented by meta-GGAs that additionally employ the orbital kinetic energy density:

$$\tau(\mathbf{r}) = \frac{1}{2}\sum_i^{occ}|\nabla\phi_i(\mathbf{r})|. \tag{1.13}$$

The functionals on the first three rungs are often called semi-local functionals. At the fourth rung of Jacob's ladder, hyper-GGAs [9] add another ingredient, the exact

exchange energy density $e_X^{HF}(\mathbf{r})$. In the conventional gauge [10, 11], it is constructed as:

$$e_{\mathrm{x}}^{\mathrm{HF}}(\mathbf{r}_1) \;=\; -\frac{1}{2}\sum_{ij}\phi_i^*(\mathbf{r}_1)\phi_j(\mathbf{r}_1)\int\frac{\phi_j^*(\mathbf{r}_2)\phi_i(\mathbf{r}_2)}{|\mathbf{r}_1-\mathbf{r}_2|}d\mathbf{r}_2. \qquad (1.14)$$

and obeys the following relationship (see Eq. (1.9)):

$$E_{\mathrm{x}}^{\mathrm{HF}} \;=\; \int e_{\mathrm{x}}^{\mathrm{HF}}(\mathbf{r})d\mathbf{r}. \qquad (1.15)$$

From Eq. (1.14), we can see that hyper-GGAs additionally depend on the occupied KS orbitals. The fifth level of Jacob's ladder, the generalized random phase approximation (RPA) [12, 13, 14, 15] is represented by functionals of all KS orbitals, both occupied and unoccupied. Such functionals are not in wide use yet.

Chapter 2

Hybrid exchange–correlation functionals

2.1 Global hybrid functionals

Hybrid exchange-correlation functionals include some admixture of the exact-exchange energy.

Global hybrid functionals are the simplest hybrid functionals that include a fixed fraction c_{HF} of exact exchange, as proposed first by Becke [16, 17]:

$$E_{xc} = c_{HF}E_x^{HF} + (1 - c_{HF})E_x^{DFA} + E_c^{DFA} \tag{2.1}$$

with fixed mixing coefficient c_{HF}. The coefficient c_{HF} is usually fitted to the experimental data. For example, PBEh [18, 19] is a popular global hybrid that has the following form

$$E_{xc} = \frac{1}{4}E_x^{HF} + \frac{3}{4}E_x^{PBE} + E_c^{PBE}. \tag{2.2}$$

This functional has substantially lower error in heats of formation and barrier heights than the corresponding semi-local functional, PBE. Because of their improved accuracy, global hybrids, such as PBEh or B3LYP [20], are widely used in electronic structure theory.

However, global hybrids are not flexible enough to describe different aspects of electronic structure simultaneously. For instance, 25% of exact exchange in the PBEh is the optimal amount for the prediction of enthalpies of formation. However, 50%

is necessary to describe barrier heights of chemical reactions well.

Another drawback of the global hybrid functionals is the incorrect behavior of the exchange potential in finite systems [21, 22]. The true exchange potential has the following asymptotic behavior:

$$v_{\mathrm{x}}(\mathbf{r})|_{r\to\infty} = -\frac{1}{r} + C \qquad (2.3)$$

where $|\mathbf{r}| = r$, while the exchange potential of the hybrid functional decays as $-c_{\mathrm{HF}}/r$. The incorrect asymptotic behavior leads to errors in describing polarizabilities of long chains [23, 24], charge transfer, and Rydberg excitations [25].

The conventional hybrid functionals are also difficult to apply for periodic systems, because the addition of exact exchange drastically increases the computational cost. Moreover, it is known that the long-range part of exact exchange is partially cancelled by correlation in metallic and small band-gap systems [26, 27]. But semilocal correlation functionals fail to describe that effect.

2.2 Range-separated hybrid functionals

Range-separated hybrids, pioneered by Savin and co-workers, represent the next generation of hybrid functionals. These functionals partition the Coulomb operator into short-range (SR) and long-range (LR) components:

$$\frac{1}{r_{12}} = \underbrace{\frac{\mathrm{erfc}(\omega r_{12})}{r_{12}}}_{\mathrm{SR}} + \underbrace{\frac{\mathrm{erf}(\omega r_{12})}{r_{12}}}_{\mathrm{LR}}, \qquad (2.4)$$

where ω is the screening parameter, $\mathbf{r}_{12} = \mathbf{r}_1 - \mathbf{r}_2$, and $r_{12} = |\mathbf{r}_{12}|$. When $\omega \to 0$, the long-range part of the interaction vanishes. Using the partitioned Coulomb operator, we can split DFA and HF exchange energy as:

$$E_x^{\text{DFT}} = E_x^{\text{SR,DFT}} + E_x^{\text{LR,DFT}} \tag{2.5}$$

$$E_x^{\text{HF}} = E_x^{\text{SR,HF}} + E_x^{\text{LR,HF}} \tag{2.6}$$

There are two major classes of range-separated hybrids: screened hybrids and long-range corrected functionals.

Screened hybrids retain only the short-range part of exact exchange. This dramatically lowers the cost of calculation for periodic systems. Heyd, Scuseria, and Ernzerhof [28] have proposed an HSE screened hybrid functional that has the following form:

$$E_{\text{xc}}^{\text{HSE}} = c_{\text{HF}} E_x^{\text{HF,SR}}(\omega) + (1 - c_{\text{HF}}) E_x^{\omega\text{PBE,SR}}(\omega)$$
$$+ E_x^{\omega\text{PBE,LR}}(\omega) + E_c^{\text{PBE}}, \tag{2.7}$$

where $E_x^{\text{HF,SR}}$ is the short-range HFx (SR-HFx), $E_x^{\omega\text{PBE,SR}}$ and $E_x^{\omega\text{PBE,LR}}$ are respectively the short- and long-range components of the PBE exchange functional [8], $c_{\text{HF}} = 1/4$ is the HF mixing parameter [29], and E_c^{PBE} is the PBE correlation functional [8]. For $\omega = 0$, HSE reduces to the conventional hybrid PBEh, also known as PBE0 [18] or PBE1PBE [19]. For $\omega \to \infty$, HSE reduces to the semi-local PBE functional. For a finite value of ω, HSE can be regarded as an interpolation between

these two limits. The value of the screening parameter $\omega = 0.11 \text{Bohr}^{-1}$ was determined by fitting to experimental band gaps [30]. HSE substantially improves the quality of band gap prediction. For thermochemistry of molecules, HSE and PBEh show very similar results.

The other class of range separated hybrids uses long-range exact exchange and short-range DFT exchange. Such functionals are called long-range corrected functionals. The long-range corrected PBE (LC-ωPBE) functional [31] has the following form:

$$E_{\text{xc}}^{\text{LC}-\omega\text{PBE}} = E_{\text{x}}^{\omega\text{PBE,SR}}(\omega) + E_{\text{x}}^{\omega\text{HF,LR}}(\omega) + E_{\text{c}}^{\text{PBE}}. \qquad (2.8)$$

LC-ωPBE and related functionals are remarkably accurate for both enthalpies of formation and barrier heights [31, 32]. Further, such methods perform well for processes involving long-range charge transfer, Rydberg excitations, and other properties that require the accurate description of the asymptotic exchange potential [25, 23, 33, 34].

The advantages of screened hybrid functionals and long-range corrected functionals were united in the HISS functional of Henderson, Izmaylov, Scuseria, and Savin [35, 36]. HISS is based on a three-range partitioning of the Coulomb potential into the short-range, middle-range, and long-range parts. HISS uses a combination of semi-local DFT exchange with the middle-range exact exchange. HISS performs simultaneously well for thermochemistry, barrier heights, and band gaps.

2.3 Local hybrids

Conventional hybrid functionals use a fixed, universal fraction of exact exchange. However, we expect that different regions in a molecule need different fractions of exact exchange. We can tune the amount of exact exchange for each specific system if we use a position-dependent fraction of exact exchange. Such functionals are called local hybrids and defined as:

$$E_{\text{xc}}^{\text{Lh}} = E_{\text{c}}^{\text{DFT}} + \int \left[f(\mathbf{r}) e_{\text{x}}^{\text{HF}}(\mathbf{r}) + (1 - f(\mathbf{r})) e_{\text{x}}^{\text{DFT}}(\mathbf{r}) \right] d^3 \mathbf{r}. \tag{2.9}$$

Here $e_{\text{x}}^{\text{DFT}}(\mathbf{r})$ and $e_{\text{x}}^{\text{HF}}(\mathbf{r})$ are the semi-local DFT exchange energy density and the exact exchange energy density, respectively. The function $f(\mathbf{r})$ in Eq. (1.14) is called a mixing function. Local hybrid functional was first introduced by Burke and coworkers [10] in 1998, but without a specific form of $f(\mathbf{r})$. Jaramillo and co-workers [6, 37] proposed and implemented a local hybrid with the following mixing function:

$$f(\mathbf{r}) = \frac{\tau_{\text{W}}(\mathbf{r})}{\tau(\mathbf{r})}, \tag{2.10}$$

$$\tau_{\text{W}}(\mathbf{r}) = \frac{|\nabla \rho(\mathbf{r})|^2}{8 \rho(\mathbf{r})}. \tag{2.11}$$

In one-electron regions, where HF exchange is the exact exchange-correlation functional, this mixing function becomes equal to one. In the homogeneous electron gas, $\nabla \rho(\mathbf{r})$ and $f(\mathbf{r})$ are 0, so that only semi-local DFT exchange is used. Unfortunately, this local hybrid shows very poor thermochemical results [37]. Later, Kaupp and coworkers [38, 39, 40] demonstrated that empirically parameterized mixing functions

including

$$f(\mathbf{r}) = \alpha \, \frac{\tau_{\mathrm{W}}(\mathbf{r})}{\tau(\mathbf{r})}, \tag{2.12}$$

(where α is an empirical parameter) provide accurate thermochemistry and reaction barriers in local hybrids of LSDA exchange.

2.4 Exchange hole and its relation to hybrid functionals

Another way to look at the different classes of hybrid functionals is in terms of the exchange hole. The exchange hole $h_{\mathrm{x}}(\mathbf{r}_1; \mathbf{r}_{12})$ is defined as:

$$E_{\mathrm{x}} = \frac{1}{2} \int \frac{\rho(\mathbf{r}_1) h_{\mathrm{x}}(\mathbf{r}_1; \mathbf{r}_{12})}{|\mathbf{r}_{12}|} d^3\mathbf{r}_1 d^3\mathbf{r}_{12} \tag{2.13}$$

The exact exchange hole is written as:

$$h_{\mathrm{x}}(\mathbf{r}_1; \mathbf{r}_{12}) = -\frac{1}{2} \frac{|\sum_i^{\mathrm{occ}} \phi_i(\mathbf{r}_1)\phi_i(\mathbf{r}_2)|^2}{\rho(\mathbf{r}_1)} \tag{2.14}$$

The exchange hole of the conventional hybrid functional can be written as:

$$h_{\mathrm{x}}^{\mathrm{Hybrid}}(\mathbf{r}_1; \mathbf{r}_{12}) = (1 - c_{\mathrm{HF}}) h_{\mathrm{x}}^{\mathrm{DFA}}(\mathbf{r}_1; \mathbf{r}_{12}) + c_{\mathrm{HF}} h_{\mathrm{x}}^{\mathrm{HF}}(\mathbf{r}_1; \mathbf{r}_{12}) \tag{2.15}$$

where c_{HF} is a constant. In a local hybrid functional, c_{HF} becomes a function of $\mathbf{r}_1$, so that:

$$h_{\mathrm{x}}^{\mathrm{Hybrid}}(\mathbf{r}_1; \mathbf{r}_{12}) = (1 - c_{\mathrm{HF}}(\mathbf{r}_1)) h_{\mathrm{x}}^{\mathrm{DFA}}(\mathbf{r}_1; \mathbf{r}_{12}) + c_{\mathrm{HF}}(\mathbf{r}_1) h_{\mathrm{x}}^{\mathrm{HF}}(\mathbf{r}_1; \mathbf{r}_{12}) \tag{2.16}$$

Similarly, the exchange hole of range-separated hybrids is written as:

$$h_{\mathrm{x}}^{\mathrm{Hybrid}}(\mathbf{r}_1; |\mathbf{r}_{12}|) = (1 - c_{\mathrm{HF}}(|\mathbf{r}_{12}|)) h_{\mathrm{x}}^{\mathrm{DFA}}(\mathbf{r}_1; \mathbf{r}_{12}) + c_{\mathrm{HF}}(\mathbf{r}_{12}) h_{\mathrm{x}}^{\mathrm{HF}}(\mathbf{r}_1; \mathbf{r}_{12}). \tag{2.17}$$

In particular, in long-range corrected functionals $c_{\mathrm{HF}}(|\mathbf{r}_{12}|) = \mathrm{erf}(\omega|\mathbf{r}_{12}|)$.

2.5   Aim of the present work

In the current work, we propose two novel approaches that use even more general expression $c_{HF}(\mathbf{r}_1, |\mathbf{r}_{12}|)$. In the first approach, discussed in Chapter 3, we introduce the long-range corrected functional that uses a position-dependent screening function rather than fixed screening parameter. In the second approach (Chapter 4), we combine local hybrid and range separation, so that we admix locally screened exchange. Both of these methods provide extra flexibility for the description of electronic structure.

Chapter 3

Hybrid functionals with local range separation

3.1 Theory

Range-separated hybrid functionals offer a promising route for the construction of accurate density functionals. However, most previous implementations of range separation use a universal, system-independent screening parameter in Eq. (2.4). It seems obvious that such an approach, despite its success, will have limitations. It has been argued that the screening parameter should rather be system-dependent [41, 42, 43, 44]. In this work, we describe an even more general approach. In the homogeneous electron gas, the size of the exchange hole measured, e.g., by the point where its first node appears, varies with the density of the gas. Therefore, it seems evident that the separation between the short-range and long-range interactions for an inhomogeneous system should depend on the local density. Here, we propose an approximation that uses a position-dependent screening function $\omega(\mathbf{r})$ defining a *local* range separation (LRS) for mixing exact (HF-type) and LSDA exchange. Our approach is presented in detail below.

3.1.1 Physical idea

We propose the following form for the exchange-correlation energy of a spin-unpolarized density:

$$E_{\text{xc}}^{\text{LRS-}\omega\text{LSDA}} = \int [e_{\text{x}}^{\text{LSDA,SR}}(\mathbf{r}, \omega(\mathbf{r})) + e_{\text{x}}^{\text{HF,LR}}(\mathbf{r}, \omega(\mathbf{r}))]\, d\mathbf{r} + E_{\text{c}}^{\text{LSDA}}, \qquad (3.1)$$

We will refer to this locally range-separated functional as LRS-ωLSDA. Eq. (3.1) is readily extended to spin-polarized systems using the spin-scaling relationship from Eq. (1.10) for the exchange energy [5] (with a different $\omega(\mathbf{r})$ for each spin component). When ω is universal and position-independent, this functional reduces to long-range corrected LSDA [45, 46], which we will here refer to as LC-ωLSDA. Note that in Ref. [45], this functional is denoted RSHXLDA. Toulouse *et al.* [47] have suggested using a local screening parameter ω for DFT correlation. We here explore an LRS approach for exchange only; our aim is to combine it with LRS correlation at a later stage.

3.1.2 Approximations for the local screening function

The realization and implementation of Eq. (3.1) is non-trivial. One should choose an appropriate screening function $\omega(\mathbf{r})$. There are several straightforward choices for the local screening parameter. In the homogeneous electron gas, a characteristic length is given by the Wigner-Seitz radius $r_s = (4\pi\rho/3)^{-1/3}$. The screening parameter has dimensions of inverse length, so a trivial selection would be $\omega(\mathbf{r}) \sim 1/r_s$ [47, 48]. For

inhomogeneous systems, the screening function can be approximated by a gradient expansion:

$$\omega(\mathbf{r}) = \frac{1}{r_s}(\alpha + \beta s + \gamma s^2 + \ldots), \tag{3.2}$$

where $s = |\nabla\rho|/(2k_F\rho)$ is the reduced gradient, $k_F = (3\pi^2\rho)^{1/3}$, and α, β, and γ are parameters to be determined. In the high-density limit, these choices for $\omega(\mathbf{r})$ have a better scaling behavior than constant ω (see Appendix A).

3.1.3 Models for the SR and LR parts of the exchange energy

The short-range component can be calculated as:

$$e_{\mathrm{x}}^{\mathrm{LSDA,SR}}(\mathbf{r}, \omega(\mathbf{r})) = \frac{1}{2}\rho(\mathbf{r})\int_0^\infty h_x^{\mathrm{LSDA}}(\rho(\mathbf{r}), u)\frac{\mathrm{erfc}(\omega(\mathbf{r})u)}{u}4\pi u^2 du, \tag{3.3}$$

where $h_x^{\mathrm{LSDA}}(\rho(\mathbf{r}), u)$ is the LSDA exchange hole and erfc(x) = 1 - erf(x). This integral can be done analytically for any value of ω [49, 50]. Note that even though Eq. (3.3) is not symmetric with respect to interchange of electrons, it does not violate symmetry invariance of the total exchange energy, as explained in Appendix B.

The long-range part (in the conventional gauge [11]) is defined as:

$$e_{\mathrm{x}}^{\mathrm{HF,LR}}(\mathbf{r}, \omega(\mathbf{r})) = \sum_{\mu\nu} \phi_\mu(\mathbf{r})\phi_\nu(\mathbf{r})\, X_{\mu\nu}^{\mathrm{LR}}(\mathbf{r}, \omega(\mathbf{r})), \tag{3.4}$$

where ϕ_μ and ϕ_ν are atomic orbitals (AOs) and

$$X_{\mu\nu}^{\mathrm{LR}}(\mathbf{r}, \omega(\mathbf{r})) = -\frac{1}{2}\sum_{\lambda\sigma} P_{\mu\lambda}P_{\nu\sigma}V_{\lambda\sigma}^{\mathrm{LR}}(\mathbf{r}, \omega(\mathbf{r})), \tag{3.5}$$

where $\mathbf{P}$ is the density matrix and $V_{\lambda\sigma}^{\mathrm{LR}}$ are Coulomb-type electrostatic integrals (ESIs):

$$V_{\lambda\sigma}^{\mathrm{LR}}(\mathbf{r}, \omega(\mathbf{r})) = \int \phi_\lambda(\mathbf{r}')\phi_\sigma(\mathbf{r}')\frac{\mathrm{erf}(\omega(\mathbf{r})|\mathbf{r} - \mathbf{r}'|)}{|\mathbf{r} - \mathbf{r}'|}d\mathbf{r}', \tag{3.6}$$

where ϕ_λ are Gaussian basis functions. These integrals can be done analytically for any $\omega(\mathbf{r})$ (see Appendix C). The long-range Fock exchange matrix may be evaluated from Eq. (3.6) as

$$K_{\mu\nu}^{\mathrm{LR}}(\omega(\mathbf{r})) = -\sum_{\lambda\sigma} P_{\lambda\sigma} \int \phi_\mu(\mathbf{r})\phi_\lambda(\mathbf{r})V_{\sigma\nu}^{\mathrm{LR}}(\mathbf{r}, \omega(\mathbf{r}))d\mathbf{r} \tag{3.7}$$

and the LR exchange energy is evaluated as

$$E_{\mathrm{x}}^{\mathrm{HF,LR}} = \int e_{\mathrm{x}}^{\mathrm{HF,LR}}(\mathbf{r}, \omega(\mathbf{r}))d\mathbf{r} = \frac{1}{2}\sum_{\mu\nu} K_{\mu\nu}^{\mathrm{LR}}(\omega(\mathbf{r}))\, P_{\mu\nu} \tag{3.8}$$

Unfortunately, these expressions are computationally intractable as written. Given an arbitrary $\omega(\mathbf{r})$, the integral over $\mathbf{r}$ in Eq. (3.7) must be performed numerically. There are $\mathcal{O}(N_{\mathrm{AO}}^2)$ matrix elements of $V_{\sigma\nu}^{\mathrm{LR}}(\mathbf{r}, \omega(\mathbf{r}))$ to be evaluated at each grid point $\mathbf{r}$, yielding a total computational cost $\mathcal{O}(N_{\mathrm{grid}}N_{\mathrm{AO}}^2)$. On the other hand, if $\omega(\mathbf{r})$ is constant, the integral over $\mathbf{r}$ in Eq. (3.7) can be performed analytically in a Gaussian basis set, leading to

$$K_{\mu\nu}^{\mathrm{LR}}(\omega) = -\sum_{\lambda\sigma}(\mu\lambda, \nu\sigma)_\omega P_{\lambda\sigma} \tag{3.9}$$

and

$$E_{\mathrm{x}}^{\mathrm{HF,LR}} = \frac{1}{2}\sum_{\mu\nu\lambda\sigma}(\mu\lambda, \nu\sigma)_\omega P_{\mu\nu}P_{\lambda\sigma} \tag{3.10}$$

where

$$(\mu\lambda, \nu\sigma)_\omega = \int\int \phi_\mu(\mathbf{r})\phi_\lambda(\mathbf{r})\frac{\mathrm{erf}(\omega|\mathbf{r} - \mathbf{r}'|)}{|\mathbf{r} - \mathbf{r}'|}\phi_\nu(\mathbf{r}')\phi_\sigma(\mathbf{r}')d\mathbf{r}d\mathbf{r}' \tag{3.11}$$

Such analytic two-electron integrals are an essential part of Gaussian-orbital based electronic structure programs. For screened interactions, the integrals in Eq. (3.11) can be evaluated as a trivial modification of regular two-electron integrals [49, 51]. While their computational scaling is formally $\mathcal{O}(N_{AO}^4)$, they quickly reach their classical $\mathcal{O}(N_{AO}^2)$ asymptote for moderate size systems [52], and a variety of linear-scaling treatments have been developed for large systems [53]. Of course for $\omega \to \infty$, all these expressions recover their exact values for the bare unscreened interaction.

As explained in detail below, an approximation to the screened HF exchange energy density is needed for computational convenience. An alternative approach for calculating the HF exchange energy density is the method of Della Salla and Görling [54]. In this method, which we here extend for using with screened interactions, the expression for the HF exchange energy density is simplified by introducing a resolution-of-the-identity (RI) in an auxiliary basis identical to the AO basis, and leads to the following expansion:

$$e_x^{HF,LR}(\mathbf{r}, \omega) = \sum_{\mu\nu} \phi_\mu(\mathbf{r})\phi_\nu(\mathbf{r})\, Q_{\mu\nu}^{LR}(\omega) \qquad (3.12)$$

where

$$\mathbf{Q}^{LR}(\omega) = \frac{1}{2}\mathbf{S}^{-1}\, \mathbf{K}^{LR}(\omega)\, \mathbf{P} + \frac{1}{2}\mathbf{P}\, \mathbf{K}^{LR}(\omega)\, \mathbf{S}^{-1}. \qquad (3.13)$$

and $\mathbf{S}^{-1}$ is the inverse overlap matrix. Note the similarities between Eqs. (3.4) and (3.12). However, also note that while $\mathbf{X}$ depends explicitly on $\mathbf{r}$, $\mathbf{Q}$ is independent of it, except through $\omega(\mathbf{r})$. The former is exact whereas the latter is approximate.

Given $\mathbf{Q}$, Eq. (3.12) can readily be evaluated at every grid point with minimal

computational cost. While the orbital product $\phi_\mu(\mathbf{r})\phi_\nu(\mathbf{r})$ decays exponentially with increasing distance between AOs, the Coulomb-type ESIs of Eq. (3.6) do not decay as fast. Thus, for constant ω (including $\omega \to \infty$, i.e., the bare interaction), RI is usually preferred over ESIs for calculating $e_x^{\mathrm{HF,LR}}(\mathbf{r},\omega)$ because of its lower computational cost [55]. Note that an important savings consideration in RI is that for constant ω, $\mathbf{K}$ (needed for $\mathbf{Q}$) can be obtained analytically via modified two-electron integrals, Eq. (3.9).

For a local screening function $\omega(\mathbf{r})$, $\mathbf{K}$ can no longer be evaluated analytically and has to be done numerically via Eq.(3.7), which involves evaluation of ESIs, so the computational advantage of RI disappears. In summary, with LRS, both the RI and exact ESI procedures have similarly steep computational costs, requiring an $\mathcal{O}(N_{grid}N_{\mathrm{AO}}^2)$ computational step that we wish to avoid. Therefore, we shall seek an alternative approximation for evaluating $e_x^{\mathrm{HF,LR}}(\mathbf{r},\omega(\mathbf{r}))$ whose computational cost is not much larger than evaluating the unscreened ($\omega \to \infty$) HF exchange energy density, which can be efficiently done via RI.

Let's recall that the TPSS exchange hole [56] was constructed to reproduce the TPSS exchange energy density:

$$e_x^{\mathrm{TPSS}}(\mathbf{r}) = \frac{1}{2}\rho(\mathbf{r}) \int_0^\infty \frac{h_x^{\mathrm{TPSS}}(\rho, |\nabla\rho|, \tau, e_x^{\mathrm{TPSS}}, u)}{u} 4\pi u^2 du \qquad (3.14)$$

where $h_x^{\mathrm{TPSS}}(\rho, |\nabla\rho|, \tau, e_x^{\mathrm{TPSS}}, u)$ is the model TPSS exchange hole [56] and τ the kinetic energy density. To achieve this goal, the TPSS hole expression has e_x^{TPSS} as an ingredient. We propose here to use the TPSS hole expression for reproducing

the screened HF exchange energy density. We feed in the unscreened e_x^{HF} instead of e_x^{TPSS} in the above equation, and integrate with the screened interaction, to yield the following approximation:

$$e_x^{HF,LR}(\mathbf{r}, \omega(\mathbf{r})) \approx \frac{1}{2}\rho(\mathbf{r}) \int_0^\infty h_x^{TPSS}(\rho, |\nabla\rho|, \tau, e_x^{HF}, u)\frac{\text{erf}(\omega(\mathbf{r})u)}{u}4\pi u^2 du \qquad (3.15)$$

For $\omega \to \infty$, Eq. (3.15) is exact. The accuracy of this approximation is examined in the Section 3.2. Note that the conventional gauge of the HF energy density e_x^{HF} in Eq. (3.4) differs slightly from the gauge of the TPSS energy density e_x^{TPSS}, as studied in Ref. [11], leading to a small error in Eq. (3.15) even when the integrated HF and TPSS exchange energies are equal for good reason. Because the TPSS exchange hole is based on the PBE hole model, the integral in Eq. (3.15) can be done (mostly) analytically, as shown in Refs. [28] and [57]. This yields a procedure with rather moderate computational cost compared to the numerical integration alternatives via RI and ESIs discussed above. A recently redeveloped PBE hole model [58] can be extended to include the exchange energy density as an ingredient (resembling the TPSS hole) and still afford exact (as opposed to "mostly") analytic integration for screened interactions.

The fourth or hyper-GGA (generalized gradient approximation) rung introduces the exact exchange energy density. From the perspective of ladder approximations and even though not explicit from the expressions in Eqs. (3.4)-(3.6), range-separated hybrids introduce further ingredients, minimally the spherically-averaged exact exchange hole density $h_x^{ex}([\rho]; \mathbf{r}, u)$, and thus stand at least slightly higher than the

fourth rung. In our actual implementation of Eq. (3.1), by using Eq. (3.15) we are making a hyper-GGA approximation to a range-separated hybrid.

3.2   Results and discussion

We have implemented LRS-ωLSDA into the development version of the Gaussian suite of programs [59]. All benchmark calculations were performed non-self-consistently using LSDA orbitals. For LSDA correlation, we use the Perdew-Wang parametrization [60]. The unscreened HF exchange energy density, needed as an ingredient for Eq. (3.15), is calculated using the RI method (see Eq. (3.12)) [54]. This method works best with large and uncontracted basis sets, so we have used the uncontracted 6-311++G(3df,3pd) basis set unless otherwise specified. When presenting our results, we employ the convention: error = theory − experiment. Unless specified otherwise, we use B3LYP/6-31G(2df,p) equilibrium geometries and zero-point energies for all species. Thermal corrections are calculated with a frequency scale factor 0.9854.

The performance of our approximate expression for the locally screened LR HF exchange energy, Eq. (3.15), can be calibrated in a benchmark case where we know the correct answer. In Fig. 1 we plot mean absolute errors (MAE) in enthalpies of formation as a function of ω for LC-ωLSDA and the same functional evaluating the LR HF exchange energy density using the TPSS exchange hole approximation of Eq. (3.15) instead of the rigorous expression of Eq. (3.10). Results presented in
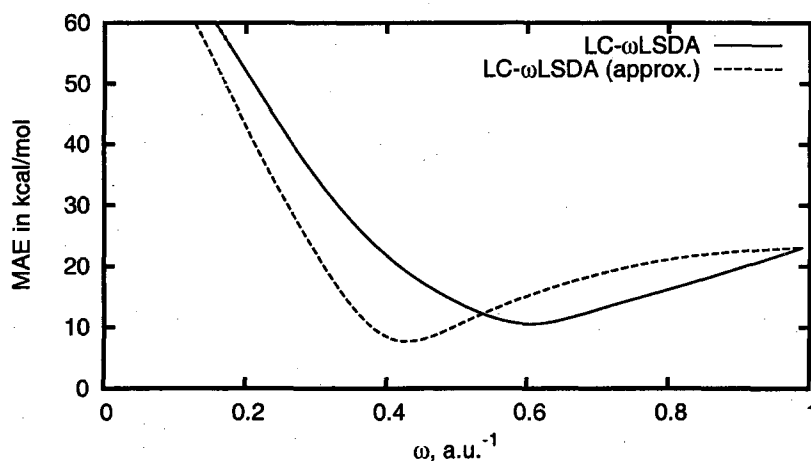
Figure 3.1 : Mean absolute errors for the standard enthalpies of formation of the AE6 set for exact and approximate LC-ωLSDA using Eq. (3.15) for $e_x^{HF,LR}(\mathbf{r}, \omega(\mathbf{r}))$.

Fig. 1 are post-LSDA (i.e., done with LSDA orbitals) and we use the AE6 test set of standard enthalpies of formation [61]. This test set includes only 6 molecules, but it has been constructed to reproduce the errors of the much larger G3 set [62].

The "exact" LC-ωLSDA in Fig. 1 shows the lowest MAE of 10.5 kcal/mol for $\omega = 0.60$. Best results with the approximate LC-ωLSDA are achieved with $\omega = 0.40$, where the MAE is 8.4 kcal/mol. Therefore, we conclude that Eq. (3.15) yields reasonably accurate results for thermochemistry, even though the optimal screening parameters are different. Note also that these optimal values would slightly change if obtained with self-consistent orbitals as opposed to the post-LSDA procedure used here.

In order to test the proposed LRS-ωLSDA approach, we use Eq. (3.2) for the local screening parameter. We have explored the parameter space for α, β, and γ in Eq. (3.2). Our current attempts indicate that optimal results are achieved with

Table 3.1 : Deviation from the experiment of standard enthalpies of formation for LRS-ωLDA. AE6 test was used. All values are in kcal/mol.

Method	$\omega(\mathbf{r})$	η	MAE
LDA			77.7
LC-ωLDA	0.6		10.6
LRS-ωLDA	η/r_s	1	24.2
LRS-ωLDA	ηs	0.29	6.6
LRS-ωLDA	$\eta s^2/r_s$	0.3	5.4
LRS-ωLDA	$\eta|\nabla\rho|/\rho$	0.135	3.6
HF exch + LDA corr			50.8

$\alpha, \gamma \approx 0$. We can then rewrite Eq. (3.2) in terms of the density and its gradient:

$$\omega(\mathbf{r}) = \frac{\beta\, s}{r_s} = \frac{\eta\,|\nabla\rho|}{\rho} \qquad (3.16)$$

where $\eta = (18\pi)^{-1/3}\beta$. This choice of screening function was previously proposed by Toulouse et al. [47] In Table 3.1, we present results for the AE6 test set of standard enthalpies of formation with several versions of LRS-ωLSDA and related functionals. For each $\omega(\mathbf{r})$ approximation, we show the optimal value of the scaling parameter η and corresponding MAE. Note that LC-ωLSDA data in this and all subsequent tables are calculated with screening parameter $\omega = 0.60$. The lowest MAE in Table 3.1 is achieved with $\omega(\mathbf{r})$ given by Eq. (3.16) and $\eta = 0.135$.

Plots of $|\nabla\rho|/\rho$ for atoms were presented several years ago in Refs. [64] and [65]. Here, in Figs. 2 and 3, we present plots of our screening function $\omega(\mathbf{r})$ in the

Table 3.2 : Total non-relativistic energies of atoms (Hartree) with the uncontracted UGBS basis set.

Atom	LSDA	LC-ωLSDA	LRS-ωLSDA	Exact[a]
H	−0.479	−0.516	−0.501	−0.500
He	−2.834	−2.925	−2.909	−2.904
Li	−7.343	−7.443	−7.467	−7.478
Be	−14.446	−14.560	−14.621	−14.667
B	−24.354	−24.493	−24.582	−24.654
C	−37.468	−37.636	−37.742	−37.845
N	−54.134	−54.332	−54.448	−54.589
O	−74.527	−74.757	−74.895	−75.067
F	−99.110	−99.368	−99.520	−99.775
Ne	−128.230	−128.511	−128.672	−128.938
Na	−161.444	−161.729	−161.931	−162.255
Mg	−199.135	−199.420	−199.664	−199.994
Al	−241.317	−241.609	−241.893	−242.277
Si	−288.216	−288.519	−288.834	−289.281
P	−340.000	−340.319	−340.657	−341.169
S	−396.737	−397.077	−397.439	−398.013
Cl	−459.662	−459.024	−459.402	−460.042
Ar	−525.940	−526.324	−526.714	−527.420
ME/$\bar{e}$[b]	0.0062	0.0038	0.0024	
MAE/$\bar{e}$[c]	0.0062	0.0041	0.0024	

[a] [63]

[b] Mean error per electron

[c] Mean absolute error per electron
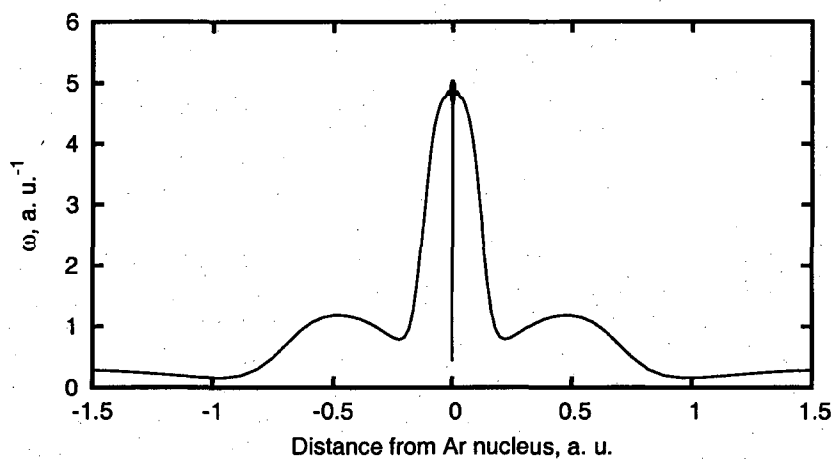
Figure 3.2 : Range separation function $\omega(\mathbf{r})$ in the argon atom, plotted as a function of the distance from nucleus.
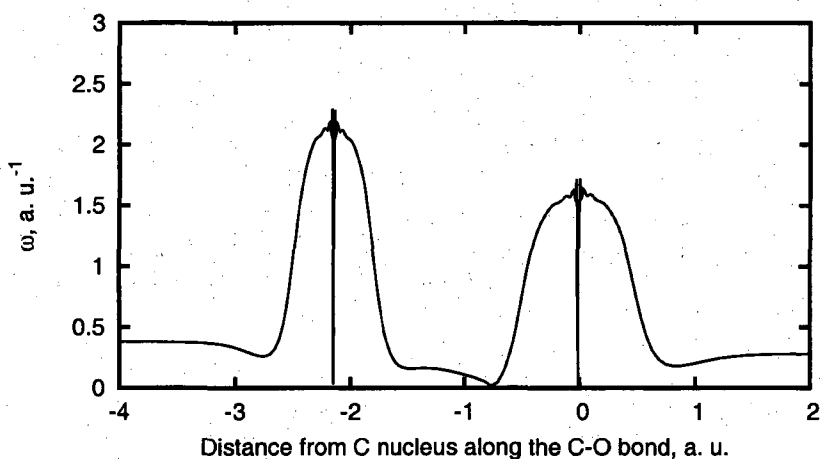
Figure 3.3 : Range separation function $\omega(\mathbf{r})$ for the majority-spin density, plotted along the bond axis of the CO molecule.

Ar atom and the CO molecule, respectively. The screening function $\omega(\mathbf{r})$ has local maxima at nuclear positions, decreases in the valence region, and increases again in the density tail. Small oscillations around the nuclei are due to the use of Gaussian basis functions.

The asymptotic behavior of $|\nabla\rho|/\rho$ is well-known. As $r \to \infty$, the density decays like [66] $Ar^{2\zeta}\exp(-2\theta r)$, where (in atomic units) $\theta = (-2\epsilon_{HOMO})^{1/2}$ and ϵ_{HOMO} is the highest-occupied (or partly occupied) orbital energy, and $\zeta = 1/\theta - 1$ for a neutral system. (For the hydrogen atom, for example, $\theta = 1$ and $\zeta = 0$.) Thus $|\nabla\rho|/\rho \to 2\theta$.

Based on the results of Table 3.1, we decided to study LRS-ωLSDA with $\omega = 0.135|\nabla\rho|/\rho$ in more detail. In Table 3.2, we present calculated atomic energies for H to Ar with the large UGBS basis set [67]. We compare LSDA, LC-ωLSDA, and LRS-ωLSDA with accurate non-relativistic energies [63]. LRS-ωLSDA has lower mean error per electron than either LSDA or LC-ωLSDA.

To assess the performance of LRS-ωLSDA for enthalpies of formation in more general cases, we have used the G3/99 test set of 223 molecules [62] and its smaller subset G2/97 of 148 molecules [68]. The results are presented in Table 3.3. LC-ωLSDA dramatically reduces MAE for the G3 test set in comparison with LSDA. However, even better results are achieved with LRS-ωLSDA that yields MAE(G3) of 5.9 kcal/mol. For thermochemistry, LRS-ωLSDA is competitive with many common hybrid functionals [69]. For comparison purposes, the popular B3LYP functional yields MAE of 3.1 and 4.9 kcal/mol for the G2 and G3 sets, respectively [69].

Table 3.4 shows benchmark results for reaction barrier heights. The HTBH38/04 set includes forward and reverse barrier heights for 19 hydrogen transfer reactions, and NTBH38/04 consists of 19 nonhydrogen-transfer reactions [70, 71]. We take the best theoretical estimates of the barrier heights and the geometries of all species from

Table 3.3 : Deviations from experiment of standard enthalpies of formation ($\Delta_f H^{\circ}_{298}$) computed with various methods using the uncontracted 6-311++G($3df,3pd$) basis set. All values are in kcal/mol.

| Functional | $\Delta_f H^{\circ}_{298}$ (kcal/mol) | | | |
| | G2 set | | G3 set | |
	ME	MAE	ME	MAE
LSDA	−83.0	83.0	−120.9	120.9
LC-ωLSDA	−2.0	10.5	−2.5	12.2
LRS-ωLSDA	−2.4	5.0	0.9	5.9

Ref. [71]. From Table 3.4, we see that LSDA substantially underestimates barrier heights. LC-ωLSDA and especially LRS-ωLSDA improve upon LSDA.

Table 3.5 presents results for ionization potentials (IP) and electronic affinities (EA) in the G2 test set [68]. We dropped the ions H_2S^+, O_2^+, NO^-, and N_2^+ from this set because of convergence issues with LSDA. In total, we used here 83 ionization potentials and 57 electron affinities. LRS-ωLSDA performs much better than either LSDA or LC-ωLSDA. Global hybrids like the popular B3LYP functional yield somewhat better MAE for IP (0.184 eV) and EA (0.124 eV) [69]. Surprisingly, the results with LC-ωLSDA are particularly poor. We have repeated the LC-ωLSDA calculations self-consistently (instead of using LSDA orbitals), and the results are only slightly better than the post-LSDA results.

Table 3.4 : Deviations from experiment of barrier heights of chemical reactions computed with various methods using the uncontracted 6-311++G($3df$,$3pd$) basis set. All values are in kcal/mol.

| Functional | $\Delta_f H_{298}^o$ (kcal/mol) | | | |
| | HTBH38 | | NHTBH38 | |
	ME	MAE	ME	MAE
LSDA	−17.9	17.9	−12.4	12.6
LC-ωLSDA	7.0	7.1	8.6	8.6
LRS-ωLSDA	−5.4	5.5	−5.3	5.5

3.3 Other approaches for construction of the local screening function

We had already demonstrated that $\omega(\mathbf{r}) = \frac{\beta}{r_s}s$ shows excellent results for both thermochemistry and barrier heights. In the last expression, we can try to substitute the reduced gradient s with the iso-orbital indicator $z = \frac{\tau_W}{\tau}$. Both of these variables are dimensionless. We obtain the following expression for the local screening function:

$$\omega(\mathbf{r}) = \beta_1 \frac{z}{r_s} \tag{3.17}$$

where $\beta_1 = 0.75$ is an empirical parameter, fitted to the small AE6 set [61] of atomization energies.

Another way to determine the screening function is to fit it, so that the semi-local part of LRS-ωLSDA reproduces the semi-local DFT part of a local hybrid functional.

Let's consider the local hybrid developed by Kaupp *et al.* [38]:

$$E_x^{FR-Lh-LSDA} = \int \left[\kappa \frac{\tau_w(\mathbf{r})}{\tau(\mathbf{r})} e_x^{HF}(\mathbf{r}) + (1 - \kappa \frac{\tau_w(\mathbf{r})}{\tau(\mathbf{r})}) e_x^{LSDA}(\mathbf{r}) \right] d\mathbf{r}. \quad (3.18)$$

where $\kappa = 0.48$ is an empirical parameter fitted to thermochemistry, and FR-Lh-LSDA stands for "full-range local hybrid of local spin-density approximation". We can reproduce its LSDA part with LRS-ωLSDA, if we choose $\omega(\mathbf{r})$ by solving the equation:

$$e_x^{LSDA,SR}(\mathbf{r}, \omega(\mathbf{r})) = (1 - \kappa_1 \frac{\tau_w(\mathbf{r})}{\tau(\mathbf{r})}) e_x^{LSDA}(\mathbf{r}) \quad (3.19)$$

Alternatively, we can reproduce the HF part of FR-Lh-LSDA, if we solve the equation:

$$e_x^{HF,LR}(\mathbf{r}, \omega(\mathbf{r})) = \kappa_2 \frac{\tau_w(\mathbf{r})}{\tau(\mathbf{r})} e_x^{HF}(\mathbf{r}) \quad (3.20)$$

where $e_x^{HF,LR}(\mathbf{r}, \omega(\mathbf{r}))$ is the approximate long-range HF energy density, calculated according to Eq. (3.15). In Eqs. (3.19) and (3.20), γ_1 and γ_2 are again empirical parameters. Both of these equations can be solved numerically at any $\mathbf{r}$, using the Newton-Raphson algorithm. This yields the screening function $\omega(\mathbf{r})$. The short-range energy density $e_x^{LSDA,SR}(\mathbf{r}, \omega(\mathbf{r}))$ can then be calculated according to Eq. (3.3). The values $\kappa_1 = 0.61$ and $\kappa_2 = 0.54$ were determined by fitting to the AE6 test set for atomization energies. In Fig. 3, we compare the different approximations for $\omega(\mathbf{r})$ in N_2 molecule.

Table 3.6 compares the performance of different approximations for $\omega(\mathbf{r})$. We see that the best results for all the test sets are achieved with $\omega(\mathbf{r}) = 0.75 \frac{z}{r_s}$. The
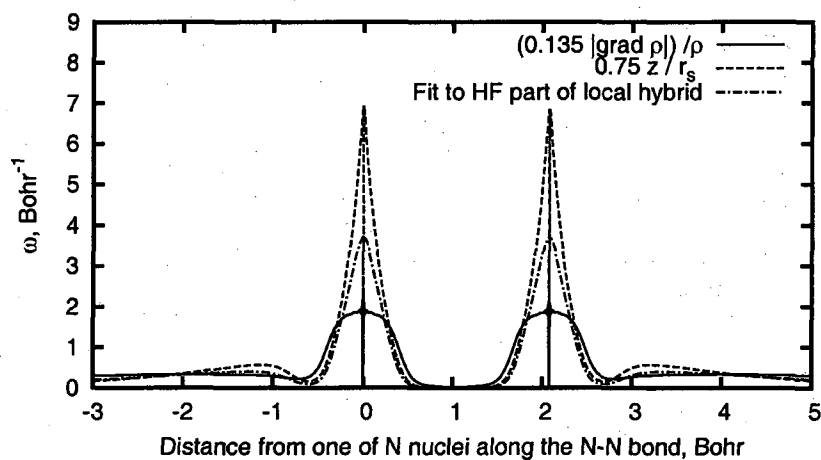
Figure 3.4 : Three different range separation functions $\omega(\mathbf{r})$ for the alpha-spin density, plotted along the bond axis of the N2 molecule.

expression $\omega(\mathbf{r}) = 0.135|\nabla\rho|/\rho$, described in detail in previous section, yields slightly worse results. But overall, all four approximations for $\omega(\mathbf{r})$ show comparable accuracy for both thermochemistry and barrier heights. It is encouraging that LRSω-LSDA always outperforms LC-ωLSDA.

Table 3.5 : Deviations from experiment of ionization potentials and electron affinities computed with various methods using the uncontracted 6-311++G($3df,3pd$) basis set. All values are in eV

Functional	IP		EA	
	ME	MAE	ME	MAE
LSDA	0.046	0.235	0.237	0.246
LC-ωLSDA	0.633	0.635	0.392	0.407
LRS-ωLSDA	0.028	0.195	0.189	0.192

Table 3.6 : MAE (mean absolute error) for test sets of enthalpies of formation ($\Delta_f H^\circ_{298}$) and barrier heights, computed with various screening functions $\omega(\mathbf{r})$. All values are in kcal/mol.

$\omega(\mathbf{r})$	$\Delta_f H^\circ_{298}$ (kcal/mol)			
	G2	G3	HTBH38	NHTBH38
$0.135\lvert\nabla\rho\rvert/\rho$	5.0	5.9	5.5	5.5
$0.75z/r_s$	4.1	5.4	4.3	5.8
Fit to DFT part of FR-Lh-LSDA	5.8	6.9	5.3	6.6
Fit to HF part of FR-Lh-LSDA	5.4	7.7	4.6	5.5

Chapter 4

Range-separated local hybrid functionals

4.1 Theory

In this chapter, we present a new combination of the local and range-separated approximations. Our "local admixture of screened exchange" partitions the exchange energy as in Eq. (2.4), with a *universal* range-separation parameter ω and a *position-dependent* admixture of SR HF exchange. This approximation complements the position-dependent ω approach described in chapter 3. We consider two limiting cases: long-range-corrected local hybrids

$$E_{xc}^{LC-Lh} = E_x^{LR-HF} + E_c^{DFA}$$

$$+ \int \left[f(\mathbf{r})e_x^{SR-HF}(\mathbf{r}) + (1 - f(\mathbf{r}))e_x^{SR-DFT}(\mathbf{r}) \right] d\mathbf{r}. \tag{4.1}$$

and screened local hybrids

$$E_x^{SC-Lh} = E_x^{LR-DFT} + E_c^{DFT}$$

$$+ \sum \int \left[f(\mathbf{r})e_x^{SR-HF}(\mathbf{r}) + (1 - f(\mathbf{r}))e_x^{SR-DFT}(\mathbf{r}) \right] d\mathbf{r}. \tag{4.2}$$

The short-range HF exchange energy density $e_x^{SR-HF}(\mathbf{r})$ in Eqs. (4.1) and (4.2) is obtained by replacing $1/|\mathbf{r}-\mathbf{r}'|$ with $\mathrm{erfc}(\omega|\mathbf{r}-\mathbf{r}'|)/|\mathbf{r}-\mathbf{r}'|$ in Eq. (1.14) (see Sec. 4.2). The short-range semilocal exchange energy density $e_x^{SR-DFT}(\mathbf{r})$ is obtained from model exchange holes as in standard range-separated hybrids [23, 72, 73, 58, 74]. LC local

hybrids incorporate 100% asymptotic HF exchange regardless of the choice of mixing function. (Mixing functions incorporating 100% asymptotic HF exchange by construction were proposed in Refs. [37, 39, 40, 75, 76]). These functionals will be valuable for calculations on finite systems, where HF exchange provides the exact asymptotic exchange-correlation potential. Screened local hybrids incorporate only SR HF exchange, regardless of the choice of mixing function. They will be essential for local hybrid treatments of metals and narrow-bandgap semiconductors, due to the aforementioned problems of LR-HF exchange in such systems [26, 27].

Range-separated local hybrids stand between the fourth and the fifth rungs of Jacob's ladder (see chapter 2). On one hand, they depend only on the occupied KS orbitals, so they are below the fifth rung. On the other hand, range-separated local hybrids use not the exact exchange energy density itself, but its screened counterpart (Eq. (3.12)), so they differ from the fourth rung. In this work, we test screened and LC local hybrids that use the empirical mixing function of Eq. (2.12) to locally admix SR HF exchange. These functionals contain two empirical parameters: the maximum fraction of SR HF exchange α in Eq. (2.12), and the universal range-separation parameter ω in Eq. (2.4).

The local, range-separated, and local-range-separated hybrid functionals discussed above are all special cases of exchange-correlation functionals that depend explicitly on the occupied Kohn-Sham spin orbitals. Self-consistent implementations of such functionals typically follow one of two routes. The first route is to calculate

the Kohn-Sham local XC potential

$$v_{\mathrm{xc}\sigma}(\mathbf{r}) = \frac{\delta E_{\mathrm{xc}}}{\delta \rho_\sigma(\mathbf{r})}, \tag{4.3}$$

using the optimized effective potential method (OEP) [77, 78, 79, 80, 81] or approximations such as KLI [82] or LHF/CEDA [54, 83]. Such calculations yield high quality one-particle spectra [79, 80] and are useful for properties such as NMR chemical shifts [84, 85, 86], but have formal and computational problems in finite basis sets [87, 88, 89, 90]. The second route is to calculate the nonlocal XC potential defined in terms of functional derivatives with respect to the spin orbitals:

$$\hat{v}_{\mathrm{xc}\sigma}\phi_{i\sigma}(\mathbf{r}) \leftarrow \frac{\delta E_{\mathrm{xc}}}{\delta \phi_{i\sigma}^*(\mathbf{r})}. \tag{4.4}$$

Eq. (4.4) contributes to the Fock-like Hamiltonian matrix in a finite KS orbital basis set $\{\mu(\mathbf{r})\}$ with matrix elements

$$V_{\mu\nu,\sigma}^{\mathrm{xc}} = \int d\mathbf{r} \; \mu^*(\mathbf{r})\hat{v}_{\mathrm{xc}\sigma}\nu(\mathbf{r}). \tag{4.5}$$

This generalized Kohn-Sham (GKS) approach is outside of the Kohn-Sham formalism, but is a rigorous generalized density functional theory in its own right [91, 92]. GKS appears to be behind the success of the HSE06 screened hybrid for semiconductor band gaps [28, 93, 94, 95]. GKS is also typically simpler to implement and more computationally tractable than OEP approximations. Most existing density functional codes use GKS implementations of hybrid and meta-GGA functionals.

Local hybrid functionals were implemented self-consistently within the LHF/CEDA approximation to OEP by Arbuznikov, Kaupp, and Bahmann in

2006 [96]. This self-consistent "localized local hybrid" (LLH) method was later extended and applied in calculations of nuclear shielding constants [97]. The implementation is computationally demanding, requiring two separate resolutions of the identity to construct the averaged local potential entering the LLH equations. Most subsequent thermochemical tests of local hybrids have been performed non-self-consistently [38, 39, 40, 75, 76, 98].

In this chapter, we present self-consistent GKS calculations using the screened and LC local hybrid functionals of Eqs. (4.1–4.2). In section 4.2, we derive the nonlocal GKS exchange potential. Section 4.3 gives details of our implementation and calculations. Section 4.4 presents thermochemical tests of screened and LC local hybrids. Section 4.4 also compares our GKS approach to published non-self-consistent and LLH treatments of existing local hybrids of full-range HF exchange.

4.2   GKS local hybrid exchange potentials

Here we derive matrix elements of the GKS exchange potential for full-range, screened, and LC local hybrid functionals. The derivation closely follows the "functional derivatives with respect to the orbitals" which were obtained by Arbuznikov and co-workers as an intermediate step in the localized local hybrids of Refs. [96, 97]. We generalize their derivation to screened exchange and complex orbitals, using partial integration to remove quantities such as $\nabla|\nabla\rho|$ and $\nabla\tau$ (see Eq. (28) of Ref. [96] and Eq. (17) of Ref. [97]). The resulting equations can also be derived following the

procedure of Pople and coworkers [99], by first expanding the KS orbitals in a basis set, then taking the partial derivative of Eq. (4.6) with respect to the expansion coefficients (not shown). Extensions to more general hyper-GGA forms are presented. We note that although the authors of Refs. [96, 97] did not report GKS calculations using the nonlocal exchange potentials constructed from their functional derivatives, they could have done so had they wished.

We begin with the exchange energy of a local hybrid of full-range HF exchange from Eq. (2.9) that we repeat here:

$$E_x^{Lh} = \int d\mathbf{r}_1 \left[f(\mathbf{r}_1) \, e_x^{HF}(\mathbf{r}_1) + (1 - f(\mathbf{r}_1)) \, e_x^{DFT}(\mathbf{r}_1) \right]. \qquad (4.6)$$

We construct the HF exchange energy density by applying a resolution of the identity (RI) to Eq. (1.14) and symmetrizing, following Della Sala and Görling [54]

$$
\begin{aligned}
e_x^{HF}(\mathbf{r}_1) &= -\frac{1}{4} \sum_{ij} \phi_i^*(\mathbf{r}_1) \int d\mathbf{s} \, \delta(\mathbf{r}_1 - \mathbf{s}) \phi_j(\mathbf{s}) \int d\mathbf{r}_2 \frac{\phi_j^*(\mathbf{r}_2)\phi_i(\mathbf{r}_2)}{|\mathbf{s} - \mathbf{r}_2|} + \text{c.c.} \qquad (4.7) \\
&= -\frac{1}{4} \sum_{ij} \sum_{\alpha\beta} \phi_i^*(\mathbf{r}_1) \alpha(\mathbf{r}_1) S_{\alpha\beta}^{-1} \int d\mathbf{s} \int d\mathbf{r}_2 \frac{\beta^*(\mathbf{s})\phi_j(\mathbf{s})\phi_j^*(\mathbf{r}_2)\phi_i(\mathbf{r}_2)}{|\mathbf{s} - \mathbf{r}_2|} + \text{c.c.}
\end{aligned}
$$

Here $\{\alpha(\mathbf{r})\}$ is the RI basis set, $S_{\alpha\beta}^{-1}$ is its inverse overlap matrix, and "c.c." denotes the complex conjugate of the displayed expression. We assume in what follows that the KS orbital basis set $\{\mu(\mathbf{r})\}$ is used for the RI. Given a spin density matrix $\mathbf{P}$ defined in terms of the occupied KS spin orbitals as

$$\sum_i \phi_i(\mathbf{r}_1)\phi_i^*(\mathbf{r}_2) = \sum_{\mu\nu} \mu(\mathbf{r}_1) P_{\mu\nu} \, \nu^*(\mathbf{r}_2), \qquad (4.8)$$

the HF exchange energy density of Eq. (4.7) becomes

$$e_x^{HF}(\mathbf{r}_1) = \frac{1}{2} \sum_{\mu\nu} \mu(\mathbf{r}_1) Q_{\mu\nu} \, \nu^*(\mathbf{r}_1), \tag{4.9}$$

$$\mathbf{Q} = \frac{1}{2} \left(\mathbf{S}^{-1} \cdot \mathbf{K} \cdot \mathbf{P} + \mathbf{P} \cdot \mathbf{K} \cdot \mathbf{S}^{-1} \right), \tag{4.10}$$

where

$$K_{\mu\nu} = -\sum_{\lambda\eta} P_{\lambda\eta} (\mu\lambda|\eta\nu), \tag{4.11}$$

$$(\mu\lambda|\eta\nu) = \int d\mathbf{r}_1 \int d\mathbf{r}_2 \frac{\mu^*(\mathbf{r}_1)\lambda(\mathbf{r}_1)\eta^*(\mathbf{r}_2)\nu(\mathbf{r}_2)}{|\mathbf{r}_1 - \mathbf{r}_2|}. \tag{4.12}$$

We assume that the local hybrid mixing function $f(\mathbf{r})$ and the exchange energy density $e_x^{DFT}(\mathbf{r})$ are real semilocal functions of $\phi_i(\mathbf{r})$, $\nabla\phi_i(\mathbf{r})$, and their complex conjugates. (Extensions to the nonlocal mixing functions of Refs. [75, 76] will be treated in future work.) $e_X^{HF}(\mathbf{r})$ is a nonlocal function of $\phi_i(\mathbf{r}')$ and $\phi_i^*(\mathbf{r}')$, but not a function of $\nabla\phi_i(\mathbf{r}')$ or $\nabla\phi_i^*(\mathbf{r}')$. Given this, the functional derivative of Eq. (4.6):

$$\frac{\delta E_x^{Lh}}{\delta\phi_i^*(\mathbf{r})} = \frac{\partial E_x^{Lh}}{\partial\phi_i^*(\mathbf{r})} - \nabla \cdot \left[\frac{\partial E_X^{Lh}}{\partial(\nabla\phi_i^*(\mathbf{r}))} \right], \tag{4.13}$$

becomes

$$\frac{\delta E_x^{Lh}}{\delta\phi_i^*(\mathbf{r})} = \left(\hat{v}^{Lh(1)} + \hat{v}^{Lh(2)} + \hat{v}^{Lh(3)} \right) \phi_i(\mathbf{r}), \tag{4.14}$$

$$\hat{v}^{Lh(1)}\phi_i(\mathbf{r}) = \int d\mathbf{r}_1 \, f(\mathbf{r}_1) \frac{\partial e_x^{HF}(\mathbf{r}_1)}{\partial\phi_i^*(\mathbf{r})}, \tag{4.15}$$

$$\hat{v}^{Lh(2)}\phi_i(\mathbf{r}) = e_{\text{diff}} \frac{\partial f(\mathbf{r})}{\partial\phi_i^*(\mathbf{r})} - \nabla \cdot \left[e_{\text{diff}} \frac{\partial f(\mathbf{r})}{\partial(\nabla\phi_i^*(\mathbf{r}))} \right], \tag{4.16}$$

$$\hat{v}^{Lh(3)}\phi_i(\mathbf{r}) = (1 - f(\mathbf{r})) \frac{\partial e_x^{DFT}(\mathbf{r})}{\partial\phi_i^*(\mathbf{r})} - \nabla \cdot \left[(1 - f(\mathbf{r})) \frac{\partial e_x^{DFT}(\mathbf{r})}{\partial(\nabla\phi_i^*(\mathbf{r}))} \right]. \tag{4.17}$$

Here

$$e_{\text{diff}} = e_x^{HF}(\mathbf{r}) - e_X^{DFT}(\mathbf{r}). \tag{4.18}$$

The nonlocal operator $\hat{v}^{\mathrm{Lh}(1)}$ is obtained by substituting Eq. (4.7) into Eq. (4.15)

$$
\begin{aligned}
\hat{v}^{\mathrm{Lh}(1)}\nu(\mathbf{r}) = -\frac{1}{4}\sum_j\sum_{\alpha\beta}\Bigg(& f(\mathbf{r})\alpha(\mathbf{r})S_{\alpha\beta}^{-1} \\
& \int d^3s\int d^3r_2\frac{\beta^*(\mathbf{s})\phi_j(\mathbf{s})\phi_j^*(\mathbf{r}_2)\nu(\mathbf{r}_2)}{|\mathbf{s}-\mathbf{r}_2|} \\
+ & \int d^3r_1\, f(\mathbf{r}_1)\nu(\mathbf{r}_1)\alpha^*(\mathbf{r}_1)\left(S_{\alpha\beta}^{-1}\right)^*\int d^3s\frac{\beta(\mathbf{s})\phi_j^*(\mathbf{s})\phi_j(\mathbf{r})}{|\mathbf{s}-\mathbf{r}|} \\
+ & \int d^3r_1\, f(\mathbf{r}_1)\phi_j^*(\mathbf{r}_1)\alpha(\mathbf{r}_1)S_{\alpha\beta}^{-1}\int d^3s\frac{\beta^*(\mathbf{s})\nu(\mathbf{s})\phi_j(\mathbf{r})}{|\mathbf{s}-\mathbf{r}|} \\
+ & \int d^3r_1\, f(\mathbf{r}_1)\phi_j(\mathbf{r}_1)\alpha^*(\mathbf{r}_1)\left(S_{\alpha\beta}^{-1}\right)^*\int d^3r_2\frac{\phi_j^*(\mathbf{r}_2)\nu(\mathbf{r}_2)\beta(\mathbf{r})}{|\mathbf{r}_2-\mathbf{r}|}\Bigg).
\end{aligned} \tag{4.19}
$$

Matrix elements of this operator are obtained from Eq. (4.5) as

$$
\begin{aligned}
V_{\mu\nu}^{\mathrm{Lh}(1)} = -\frac{1}{4}\sum_{\alpha\beta}\Bigg(& \left[\int d\mathbf{r}\,\mu^*(\mathbf{r})f(\mathbf{r})\alpha(\mathbf{r})\right]S_{\alpha\beta}^{-1} \\
& \left[\sum_j\int d\mathbf{s}\int d\mathbf{r}_2\frac{\beta^*(\mathbf{s})\phi_j(\mathbf{s})\phi_j^*(\mathbf{r}_2)\nu(\mathbf{r}_2)}{|\mathbf{s}-\mathbf{r}_2|}\right] \\
+ & \left[\sum_j\int d\mathbf{r}\int d\mathbf{s}\frac{\mu^*(\mathbf{r})\phi_j(\mathbf{r})\phi_j^*(\mathbf{s})\beta(\mathbf{s})}{|\mathbf{s}-\mathbf{r}|}\right]S_{\beta\alpha}^{-1}\left[\int d\mathbf{r}_1\alpha^*(\mathbf{r}_1)f(\mathbf{r}_1)\nu(\mathbf{r}_1)\right] \\
+ & \sum_{\lambda\eta}P_{\lambda\eta}\left[\int d\mathbf{r}_1\,\eta^*(\mathbf{r}_1)f(\mathbf{r}_1)\alpha(\mathbf{r}_1)\right]S_{\alpha\beta}^{-1}\left[\int d\mathbf{s}\int d\mathbf{r}\frac{\mu^*(\mathbf{r})\lambda(\mathbf{r})\beta^*(\mathbf{s})\nu(\mathbf{s})}{|\mathbf{s}-\mathbf{r}|}\right] \\
+ & \sum_{\lambda\eta}\left[\int d\mathbf{r}\int d\mathbf{r}_2\frac{\mu^*(\mathbf{r})\beta(\mathbf{r})\eta^*(\mathbf{r}_2)\nu(\mathbf{r}_2)}{|\mathbf{r}_2-\mathbf{r}|}\right]S_{\beta\alpha}^{-1}\left[\int d\mathbf{r}_1\,\alpha^*(\mathbf{r}_1)f(\mathbf{r}_1)\lambda(\mathbf{r}_1)\right]P_{\lambda\eta}\Bigg),
\end{aligned} \tag{4.20}
$$

where $\left(S_{\alpha\beta}^{-1}\right)^* = S_{\beta\alpha}^{-1}$ and Eq. (4.8) is invoked. Simplification yields the matrix representation of the operator

$$
\mathbf{V}^{\mathrm{Lh}(1)} = \frac{1}{4}\left(\mathbf{f}\cdot\mathbf{S}^{-1}\cdot\mathbf{K}+\mathbf{K}\cdot\mathbf{S}^{-1}\cdot\mathbf{f}\right)+\frac{1}{2}\tilde{\mathbf{K}}, \tag{4.21}
$$

where the matrix $\mathbf{f}$ is given by

$$
f_{\mu\nu} = \int d\mathbf{r}\,\mu^*(\mathbf{r})f(\mathbf{r})\nu(\mathbf{r}), \tag{4.22}
$$

and the matrix $\tilde{\mathbf{K}}$ is obtained by replacing $\mathbf{P}$ with $\left(\mathbf{P}\cdot\mathbf{f}\cdot\mathbf{S}^{-1}+\mathbf{S}^{-1}\cdot\mathbf{f}\cdot\mathbf{P}\right)/2$ in Eq. (4.11). For a global hybrid of full-range exact exchange, where $f(\mathbf{r})$ equals a constant α, the matrix $\mathbf{f}$ is α times the KS orbital basis overlap matrix $\mathbf{S}$, and $\mathbf{V}^{\text{Lh}(1)} = \alpha\mathbf{K}$, as expected.

Matrix elements of $\hat{v}^{\text{Lh}(2)}$ and $\hat{v}^{\text{Lh}(3)}$ are obtained in the usual way [100, 99]. $\hat{v}^{\text{Lh}(2)}$ is

$$
\begin{aligned}
\hat{v}^{\text{Lh}(2)}\nu(\mathbf{r}) \;=\;& e_{\text{diff}}\left(\nu(\mathbf{r})\,\frac{\partial f(\mathbf{r})}{\partial\rho(\mathbf{r})} + 2\left[\nabla\rho(\mathbf{r})\cdot\nabla\nu(\mathbf{r})\right]\frac{\partial f(\mathbf{r})}{\partial G(\mathbf{r})}\right) \\
&- \nabla\cdot\left[e_{\text{diff}}\left(2\left[\nabla\rho(\mathbf{r})\right]\nu(\mathbf{r})\,\frac{\partial f(\mathbf{r})}{\partial G(\mathbf{r})} + \frac{1}{2}[\nabla\nu(\mathbf{r})]\frac{\partial f(\mathbf{r})}{\partial\tau(\mathbf{r})}\right)\right].
\end{aligned}
\tag{4.23}
$$

where $G(\mathbf{r}) = |\nabla\rho(\mathbf{r})|^2$. Its matrix elements are obtained from Eq. (4.5), using a partial integration to remove terms in $e.g.$, ∇e_{diff} and $\nabla\tau$ resulting from the second line of Eq. (4.23)

$$
\begin{aligned}
V_{\mu\nu}^{\text{Lh}(2)} \;=\;& \int d\mathbf{r}\; e_{\text{diff}}\left(\mu^*(\mathbf{r})\nu(\mathbf{r})\frac{\partial f(\mathbf{r})}{\partial\rho(\mathbf{r})}\right. \\
&+ 2\left[\nabla\rho(\mathbf{r})\cdot\nabla\left(\mu^*(\mathbf{r})\nu(\mathbf{r})\right)\right]\frac{\partial f(\mathbf{r})}{\partial G(\mathbf{r})} \\
&\left.+ \frac{1}{2}\left[\nabla\mu^*(\mathbf{r})\cdot\nabla\nu(\mathbf{r})\right]\frac{\partial f(\mathbf{r})}{\partial\tau(\mathbf{r})}\right).
\end{aligned}
\tag{4.24}
$$

A similar derivation gives

$$
\begin{aligned}
V_{\mu\nu}^{\text{Lh}(3)} \;=\;& \int d\mathbf{r}\;(1-f(\mathbf{r}))\left(\mu^*(\mathbf{r})\nu(\mathbf{r})\frac{\partial e_{\text{x}}^{\text{DFT}}(\mathbf{r})}{\partial\rho(\mathbf{r})}\right. \\
&+ 2\left[\nabla\rho(\mathbf{r})\cdot\nabla\left(\mu^*(\mathbf{r})\nu(\mathbf{r})\right)\right]\frac{\partial e_{\text{x}}^{\text{DFT}}(\mathbf{r})}{\partial G(\mathbf{r})} \\
&\left.+ \frac{1}{2}\left[\nabla\mu^*(\mathbf{r})\cdot\nabla\nu(\mathbf{r})\right]\frac{\partial e_{\text{x}}^{\text{DFT}}(\mathbf{r})}{\partial\tau(\mathbf{r})}\right).
\end{aligned}
\tag{4.25}
$$

GKS exchange potentials for screened and long-range-corrected local hybrids are obtained by replacing the full-range exchange energy densities in Eq. (4.6) with the

corresponding short-range quantities. The SR DFT exchange energy density and its derivatives are obtained from DFT exchange hole models in the usual way [23, 72, 73, 58, 74]. The SR HF exchange terms are obtained by evaluating the two-electron integrals in Eq. (4.12) with the SR interaction in Eq. (2.4), and using these integrals to construct the $\mathbf{K}$ and $\tilde{\mathbf{K}}$ matrices entering Eq. (4.21). The long-range exchange energy density, which in the present work does not include local hybridization, contributes to the GKS exchange potential in the usual way.

This derivation is readily extended to more general hyper-GGAs [6, 7]. To illustrate, we consider a hyper-GGA for exchange:

$$E_{\mathrm{x}}^{\mathrm{HGGA}} = \int d\mathbf{r}\, e_{\mathrm{x}}^{\mathrm{HGGA}}(\mathbf{r}, [\rho(\mathbf{r}), G(\mathbf{r}), \tau(\mathbf{r}), \{e_{\mathrm{x,a}}^{\mathrm{HF}}(\mathbf{r})\}]) \qquad (4.26)$$

where $\{e_{\mathrm{x,a}}^{HF}(\mathbf{r})\}$ are the set of exact exchange energy densities evaluated with modified electron-electron interactions $\{h_{\mathrm{a}}(|\mathbf{r}-\mathbf{r}'|)\}$, and the exchange energy density is a functional of all the quantities in square brackets. (Here a indexes the different modified interactions.) Matrix elements of the GKS exchange potential become

$$V_{\mu\nu}^{\mathrm{HGGA}} = \sum_a V_{\mu\nu,a}^{\mathrm{HGGA(1)}} + V_{\mu\nu}^{\mathrm{HGGA(2)}} \qquad (4.27)$$

The nonlocal operators $V_{\mu\nu,a}^{HGGA(1)}$ are obtained from Eq. (4.21) by replacing $f(\mathbf{r})$ with $\partial(e_{\mathrm{x}}^{\mathrm{HGGA}}(\mathbf{r}))/\partial(e_{X,a}^{HF}(\mathbf{r}))$ in Eq. (4.22), and evaluating $\mathbf{K}$ and $\tilde{\mathbf{K}}$ with the modified electron-electron interaction $h_{\mathrm{a}}(|\mathbf{r}-\mathbf{r}'|)$. The other operator is obtained by replacing e_X^{DFT} with e_X^{HGGA} and setting $f(\mathbf{r}) = 0$ in Eq. (4.25).

4.3 Computational details

We have implemented the expressions in previous section into the development version of the GAUSSIAN electronic structure program [101]. The implementation is restricted to using the Kohn-Sham orbital basis set for the resolution of the identity used to construct the exact exchange energy density and its derivatives. Accordingly, all calculations use fully uncontracted Gaussian AO basis sets of augmented-triple-zeta or larger size [96, 11, 102].

Table 4.1 : Definition of the five local hybrid functionals investigated in this work.

	Functional	Range separation	ω	$f_\sigma(\mathbf{r})$
FR-Lh-BLYP*	BPW91	Full-range	–	τ_W/τ
FR-Lh-LSDA[†]	LSDA	Full-range	–	$0.48\,\tau_W/\tau$
SC-Lh-LSDA	LSDA	Screened	0.11	$0.55\,\tau_W/\tau$
LC-Lh-LSDA	LSDA	Long-range-corrected	0.18	$0.44\,\tau_W/\tau$
SC-Lh-PBE	PBE	Screened	0.11	$0.25\,\tau_W/\tau$

We test five local hybrid functionals: two previously proposed full-range (FR) local hybrids, screened and long-range-corrected local hybrids of LSDA, and a screened local hybrid of PBE. Details of the functionals are presented in Table 4.1. The functionals hybridize the BPW91 [103, 60, 104], LSDA (Vosko-Wilk-Nusair correlation functional V of Ref. [105]), range-separated LSDA [73], and range-separated [72] PBE [8] exchange functionals. The SC-Lh-LSDA screened local hybrid is an exten-

sion of the HSE06 [28, 30] screened hybrid. We selected the HSE06 $\omega = 0.11$ for local hybrids of screened exchange, as this value has been shown to provide a reasonable balance between accuracy and computational efficiency in screened hybrid calculations on solids [30]. The remaining empirical parameters of our screened and LC local hybrids were fitted to the small AE6 and BH6 sets of atomization energies and hydrogen transfer reaction barrier heights [106].

We test these functionals for heats of formation $((\Delta_f H^{\circ}_{298}))$ of the G2-1 (54 molecules) [107, 108], G2/97 (147 molecules) [109], and G3/99 (222 molecules) [62] data sets [110]; hydrogen-transfer reaction barrier heights of the HTBH38/04 set and non-hydrogen-transfer reaction barrier heights of the NHTBH38/04 set [70, 71]; bond lengths of the T-96R set [69, 111]; and atomization energies and reaction barrier heights of the small AE6 and BH6 test sets [106]. Geometries and experimental values for the HTBH38/04 and NHTBH38/04 sets are from Ref. [71]. Those for the AE6 and BH6 sets are from Ref. [106]. Experimental values for the T-96R set are from Ref. [69]. Be_2 was omitted from the T-96R set due to its van der Waals bond. Si_2 was omitted from the G2-1, G2/97, G3/99, and T-96R sets due to convergence issues. $(\Delta_f H^{\circ}_{298})$ calculations use equilibrium B3LYP/6-31G(2df,p) geometries and zero-point energies with a frequency scale factor of 0.9854, as recommended in Ref. [112]. Self-consistent GKS calculations with the HSE06 screened hybrid [28, 30], the LC-ωPBE long-range-corrected local hybrid [113], and the Perdew-Burke-Ernzerhof global hybrid (PBEh) [18, 19] are included for com-

Table 4.2 : Mean and mean absolute errors (kcal/mol) in $\Delta_f H^o_{298}$ for global and local hybrid functionals (see Table 4.1). Uncontracted 6-311++G(3df,3pd) basis set. Self-consistent GKS calculations unless noted otherwise.

Functional	G2-1		G2/97		G3/99	
	ME	MAE	ME	MAE	ME	MAE
FR-Lh-LSDA, post-LSDA	-1.2	3.6	-1.9	3.7	-1.2	3.4
FR-Lh-LSDA, GKS	-1.6	3.8	-2.6	4.2	-2.1	3.9
SC-Lh-LSDA	0.2	4.3	1.2	4.3	2.9	5.0
LC-Lh-LSDA	-1.4	3.6	-1.7	3.9	-0.5	3.9
HSE06	1.8	3.0	-1.0	4.0	-2.5	5.0
LC-ωPBE	2.0	3.5	-0.5	3.8	-1.0	4.3

parison. Open-shell systems are treated spin-unrestricted. Errors are calculated as theory-experiment.

4.4 Results and discussion

Table 4.2 presents mean (ME) and mean absolute (MAE) errors in heats of formation ($\Delta_f H^o_{298}$) for the G2 and G3 sets of small and medium-sized molecules. Results are presented for full-range, screened, and long-range-corrected local hybrids of LSDA exchange. Calculations use the uncontracted 6-311++G(3df,3pd) basis set following Refs. [75, 76]. Non-self-consistent "post-LSDA" calculations use orbitals from an LSDA global hybrid with 10% HF exchange, as in Ref. [40]. Non-self-consistent

Table 4.3 : Mean and mean absolute errors (kcal/mol) in reaction barrier heights for global and local hybrid functionals. Uncontracted aug-cc-pVQZ basis set, self-consistent GKS calculations unless noted otherwise.

Functional	HTBH38/04		NHTBH38/04	
	ME	MAE	ME	MAE
FR-Lh-LSDA, post-LSDA	-1.7	2.3	-1.2	2.5
FR-Lh-LSDA, GKS	-2.1	2.6	-1.5	2.6
SC-Lh-LSDA	-1.3	2.1	-0.9	2.2
LC-Lh-LSDA	-1.6	2.2	-0.5	2.3
HSE06	-4.3	4.3	-3.2	3.6
LC-ωPBE	-0.2	1.3	1.6	2.6

calculations with the full-range local hybrid FR-Lh-LSDA agree with the results in

Refs. [40] and [76], modulo small differences due to basis set, orbitals, and molecular

geometries. The thermochemical performance of this functional is slightly degraded

in self-consistent calculations, possibly because it was parameterized post-LSDA [38].

The long-range-corrected local hybrid gives very accurate thermochemistry, compara-

ble to the full-range local hybrid and the LC-ωPBE long-range-corrected functional.

The thermochemical performance of the screened local hybrid SC-Lh-LSDA is some-

what inferior, though still comparable to the HSE06 screened hybrid. The results

overall indicate that both screened and long-range-corrected local hybrids of LSDA

exchange can provide good thermochemical performance.

Table 4.4 : Mean and mean absolute errors (Angstrom) in bond lengths of the T-96R data set. Self-consistent GKS calculations, uncontracted aug-cc-pVQZ basis set.

Functional	ME	MAE
FR-Lh-LSDA	0.0079	0.0131
SC-Lh-LSDA	0.0076	0.0132
LC-Lh-LSDA	0.0060	0.0112
PBE	0.0188	0.0190
PBEh	0.0001	0.0089
HSE06	0.0006	0.0089
LC-ωPBE	-0.0068	0.0125

Table 4.3 presents errors in reaction barrier heights of the HTBH38/04 and NHTBH38/04 test sets [70, 71], evaluated for the functionals in Table 4.2. Calculations use the large uncontracted aug-cc-pVQZ basis. Again, the non-self-consistent results for the full-range local hybrid agree with Refs. [40] and [76] modulo differences in basis set and orbitals. This functional's performance is again slightly degraded in self-consistent calculations. Both screened and long-range-corrected local hybrids give accurate reaction barriers, with results comparable to the full-range local hybrid. It is especially notable that the SC-Lh-LSDA screened local hybrid provides comparable thermochemistry and significantly improved reaction barriers relative to the HSE06 screened hybrid. Though the results are not quite comparable to recent "middle-range" hybrids [35, 36], we feel that they are encouraging.

While local hybrids have been tested non-self-consistently for the bond lengths of radical cation dimers [37, 40, 75], we are not aware of published tests for conventional covalent bond lengths. Table 4.4 presents errors in bond lengths of the T-96R test set [69], evaluated using the uncontracted aug-cc-pVQZ basis set. All of the tested hybrid functionals are reasonably accurate for predicting bond lengths. The local hybrids tend to overestimate bond lengths relative to PBEh or HSE06, with unsigned errors comparable to the long-range-corrected hybrid LC-ωPBE. This bond length overestimation may be in part a consequence of the τ_W/τ mixing function. Ref. [40] demonstrated that this function has local maxima in the bonding regions of stretched bonds and transition states. This incorporation of additional HF exchange in stretched bonds was invoked to explain the accurate reaction barrier heights predicted by the FR-Lh-LSDA local hybrid [40]. We speculate that this additional HF exchange may also create an energetic bias towards moderately stretched bonds incorporating a few percent of HF exchange in the bonding region.

Previous investigations have shown that semilocal functions such as τ_W/τ and the density gradient can be used to construct accurate full-range local hybrids of LSDA exchange, but not of GGA exchange [40, 76]. (While the nonlocal density matrix similarity metrics presented in Ref. [76] yield improved GGA local hybrids, they are still not comparable to the best LSDA local hybrids.) Unfortunately, it appears that the performance of τ_W/τ in local hybrids of GGA exchange is not improved by hybridizing screened vs. full-range HF exchange. Table 4.5 compares our SC-

Table 4.5 : Mean absolute errors (kcal/mol) in AE6 atomization energies and BH6 barrier heights for the SC-Lh-PBE screened local hybrid of PBE exchange, its "parent" screened hybrid HSE06, and the SC-Lh-LSDA screened local hybrid of LSDA exchange. Self-consistent GKS calculations, uncontracted 6-311++G(3df,3pd) basis set.

Functional	AE6	BH6
SC-Lh-PBE	5.9	6.0
HSE06	4.9	4.9
SC-Lh-LSDA	4.8	2.4

Lh-PBE screened local hybrid of PBE exchange to its "parent" screened hybrid HSE06 [28, 30]. The table includes mean absolute errors (kcal/mol) in the small AE6 atomization energy and BH6 reaction barrier height test sets. Calculations are performed self-consistently in the uncontracted 6-311++G(3df,3pd) basis set. The SC-Lh-LSDA screened local hybrid gives thermochemistry and barrier heights that are significantly worse than HSE06. In contrast, as in Tables 4.2–4.3, the SC-Lh-LSDA screened local hybrid of LSDA exchange is comparable to HSE06 for atomization energies and better than HSE06 for reaction barrier heights.

The remainder of this section compares our self-consistent GKS method to the non-self-consistent and "localized local hybrid" (LLH) results obtained by Arbuznikov and co-wrokers in Ref. [96]. Results are presented for the FR-Lh-BLYP local hybrid of full-range HF exchange (Table 4.1). The calculations in Ref. [96] used the contracted cc-pVQZ atomic orbital basis set (g functions excluded) for the

KS orbitals and the corresponding uncontracted basis for RI. Our calculations use the uncontracted cc-pVQZ basis set (including g functions) for both KS orbitals and RI. Table 4.6 compares non-self-consistent (post-BPW91) and self-consistent atomic total energies. Our post-BPW91 total energies are ~ 1 mH above AKB, a small difference that is consistent with the difference in KS orbital basis. Our self-consistent GKS energies are ~ 2.5 mH below AKB's LLH energies. This is as expected: our uncontracted KS orbital basis has additional variational freedom, and OEP and approximate OEP calculations on many-electron systems generally give total energies somewhat above GKS (Refs. [79, 114]; see however Ref. [87]).

Table 4.6 :   Total atomic energies (Hartree) from local hybrid FR-Lh-BLYP (Table 4.1), evaluated post-BPW91 or self-consistently. Current GKS implementation vs. LLH of AKB (Ref. [96]). Other details are in the text.

| | post-BPW91 | | GKS | LLH |
	This work	AKB	This work	AKB
H	-0.5060	-0.5060	-0.5066	-0.5066
Li	-7.4842	-7.4854	-7.4866	-7.4862
Be	-14.6542	-14.6553	-14.6572	-14.6563
C	-37.8427	-37.8438	-37.8470	-37.8452
N	-54.5962	-54.5974	-54.6004	-54.5988
O	-75.0817	-75.0829	-75.0868	-75.0845
F	-99.7561	-99.7574	-99.7615	-99.7592
Na	-162.2932	-162.2947	-162.2984	-162.2956
Si	-289.3866	-289.3876	-289.3927	-289.3887
P	-341.2847	-341.2856	-341.2905	-341.2864
S	-398.1364	-398.1373	-398.1430	-398.1382
Cl	-460.1743	-460.1752	-460.1809	-460.1761

Chapter 5

Conclusion

In this work, we propose two novel approaches to combine range-separation and local hybrids. In the first approach, we introduce the local range separation where we use a position-dependent screening function instead of a fixed, system-independent screening parameter. We have developed the LRS-ωLSDA functional that uses a rather accurate approximation for the screened HF exchange energy density. We tested four different expressions for the position-dependent screening parameter. Each of them has just one empirical parameter, and they all demonstrate comparable accuracy. For thermochemistry, barrier heights, and atomic energies, LRS-ωLSDA shows substantial improvement upon LSDA and LC-ωLSDA. Also, LRS-ωLSDA satisfies the high-density scaling behavior better than LC-ωLSDA. More extensive studies of local range separation are currently under way including its self-consistent implementation which is required for evaluation of analytic energy gradients and other properties [115].

We have also developed an extension of local hybrid functionals to a local admixture of screened HF exchange. We have considered two limiting cases: screened local hybrids with LR DFT exchange and long-range-corrected local hybrids with LR exact exchange. Self-consistent GKS calculations using screened and long-range-corrected local hybrids of LSDA exchange show good results for molecular thermochemistry

and kinetics, comparable to the accuracy of corresponding full-range local hybrids. Long-range-corrected local hybrids have the correct asymptotic behavior of the exchange potential, and thus could be useful for the description of properties such as polarizabilities of long chains, charge transfer, or Rydberg excitations. Our LC-LSDA-Lh is one of the few local hybrid functionals [39] that both show very accurate performance for thermochemistry and have the exact asymptotic exchange potential. The success of our SC-LSDA-Lh screened local hybrid is also encouraging. Conventional, full-range local hybrids are difficult to apply to the metals and narrow-gap semiconductors because of the prohibitive computational cost of the LR exact exchange. SC-LSDA-Lh should be readily applicable to all solids since it includes only the SR part of exact exchange.

Appendix A

High-density limit for the range separation function

Consider uniform density scaling [116] to the high-density limit:

$$\rho(\mathbf{r}) \rightarrow \rho_\lambda(\mathbf{r}) = \lambda^3 \rho(\lambda \mathbf{r}) \text{ and } \lambda \rightarrow \infty. \tag{A.1}$$

The scaled density $\rho_\lambda(\mathbf{r})$ has the same number of electrons as $\rho(\mathbf{r})$, but is higher at the origin and more contracted around it. In this limit, in the absence of exact degeneracy of the Kohn-Sham non-interacting ground state, the exact exchange energy E_x^{ex} should emerge [117] to dominate E_{xc}:

$$\lim_{\lambda \rightarrow \infty} E_{xc}[\rho_\lambda]/E_x^{ex}[\rho_\lambda] = 1 \tag{A.2}$$

Eq. (A2) is an exact constraint on $E_{xc}[\rho]$ which can be satisfied by a hyper-generalized approximation [6, 118, 9] or by a locally range-separated hybrid. With a universal position-independent parameter ω in Eq.(3.1), however, it is incorrecly LSDA exchange that emerges instead:

$$\lim_{\lambda \rightarrow \infty} E_{xc}[\rho_\lambda]/E_x^{LSDA}[\rho_\lambda] = 1 \tag{A.3}$$

Certainly there is no reason to believe that relative corrections to the local density approximation should vanish in the high-density limit.

To achieve the correct behavior of Eq.(A2), we need $\omega(\mathbf{r})$ to scale up faster than $\lambda\omega(\lambda\mathbf{r})$. Because $s(\mathbf{r}) \rightarrow s(\lambda\mathbf{r})$ and $r_s(\mathbf{r}) \rightarrow \lambda^{-1}r_s(\lambda\mathbf{r})$, Eq. (3.2) scales up like $\lambda\omega(\lambda\mathbf{r})$, which is much more nearly correct than is an ω that does not change under scaling.

Note that uniform density scaling relations for long-range and short-range exchange are presented in Ref. [119].

Appendix B

Invariance of LRS energy with respect to interchange of electrons

We can write the exact exchange-correlation energy as:

$$E_{\mathrm{xc}} = \frac{1}{2} \int \int \frac{f(\mathbf{r}, \mathbf{r}')}{|\mathbf{r} - \mathbf{r}'|} d\mathbf{r} d\mathbf{r}' \qquad \text{(B.1)}$$

Suppose we have an approximation $f_{approx}(\mathbf{r}, \mathbf{r}')$ that does not have the exact symmetry property. We can define a symmetrized

$$f_{approx,symm}(\mathbf{r}, \mathbf{r}') = \frac{1}{2}(f_{approx}(\mathbf{r}, \mathbf{r}') + f_{approx}(\mathbf{r}', \mathbf{r})) \qquad \text{(B.2)}$$

that has exactly the same energy integral as $f_{approx}(\mathbf{r}, \mathbf{r}')$.

Appendix C

Analytic integration of LRS HF exchange energy

Let $e^{-\alpha|\mathbf{r}-\mathbf{R_1}|^2}$ be an s-type Cartesian Gaussian function centered at $\mathbf{R_1}$ with orbital exponent α. Evaluating Eq. (3.6) with Gaussian basis sets requires the calculation of the following integral:

$$V^{\mathrm{LR}}(\mathbf{r}, \omega(\mathbf{r})) = \int e^{-\alpha|\mathbf{r}'-\mathbf{R_1}|^2} e^{-\beta|\mathbf{r}'-\mathbf{R_2}|^2} \frac{\mathrm{erf}[\omega(\mathbf{r})|\mathbf{r}' - \mathbf{r}|]}{|\mathbf{r}' - \mathbf{r}|} d\mathbf{r}' \qquad (\mathrm{C}.1)$$

Using the Gaussian product rule [120], we can rewrite Eq. (C.1) as:

$$V^{\mathrm{LR}}(\mathbf{r}, \omega(\mathbf{r})) = \int \tilde{K} e^{-p|\mathbf{r}'-\mathbf{R_P}|^2} \frac{\mathrm{erf}[\omega(\mathbf{r})|\mathbf{r}' - \mathbf{r}|]}{|\mathbf{r}' - \mathbf{r}|} d\mathbf{r}' \qquad (\mathrm{C}.2)$$

where the exponent of the new Gaussian is $p = \alpha + \beta$, its center is $\mathbf{R_P} = (\alpha\mathbf{R_1} + \beta\mathbf{R_2})/(\alpha + \beta)$, and

$$\tilde{K} = e^{-(\alpha\beta/(\alpha+\beta))|\mathbf{R_1}-\mathbf{R_2}|^2} \qquad (\mathrm{C}.3)$$

The Fourier transform of the short-range potential is:

$$\frac{\mathrm{erf}(\omega|\mathbf{r}' - \mathbf{r}|)}{|\mathbf{r}' - \mathbf{r}|} = (2\pi)^{-3} \int \frac{4\pi}{k^2} e^{-\frac{k^2}{4\omega^2}} e^{i\mathbf{k}\cdot(|\mathbf{r}'-\mathbf{r}|)} d\mathbf{k} \qquad (\mathrm{C}.4)$$

Using Eq. (C.4) and substituting $1/q^2 = 1/p^2 + 1/\omega^2$, we can rewrite Eq. (C.2) as:

$$V^{\mathrm{LR}}(\mathbf{r}, \omega(\mathbf{r})) = (2\pi)^{-3} \tilde{K} \int \left(\frac{\pi}{p}\right)^{3/2} \frac{4\pi}{k^2} e^{-\frac{k^2}{4q^2}} e^{i\mathbf{k}\cdot\mathbf{r}} d\mathbf{k} \qquad (\mathrm{C}.5)$$

It is shown, e.g., in Ref. [120] that the integral in Eq. (C.5) can be obtained analytically, so that:

$$V^{\mathrm{LR}}(\mathbf{r}, \omega(\mathbf{r})) = \tilde{K} \left(\frac{\pi}{\alpha + \beta}\right)^{3/2} \frac{\mathrm{erf}(q|\mathbf{r} - \mathbf{R_P}|)}{|\mathbf{r} - \mathbf{R_P}|} \qquad (\mathrm{C}.6)$$

Bibliography

[1] P. Hohenberg and W. Kohn, Phys. Rev. **136**, B864 (1964).

[2] W. Kohn and L. J. Sham, Phys. Rev. **140**, A1133 (1965).

[3] Atomic units will be used throughout this work ($e^2 = \hbar = m_e = 1$). Also all derivations are done for the spin-unpolarized case.

[4] U. von Barth and L. Hedin, J. Phys. C: Solid State Phys. **5**, 1629 (1972).

[5] G. L. Oliver and J. P. Perdew, Phys. Rev. A **20**, 397 (1979).

[6] J. P. Perdew and K. Schmidt, in *Density Functional Theory and Its Application to Materials*, edited by V. Van Doren, C. Van Alsenoy, and P. Geerlings (American Institute of Physics, Melville, NY, 2001).

[7] J. P. Perdew, A. Ruzsinszky, J. Tao, V. N. Staroverov, G. E. Scuseria, and G. I. Csonka, J. Chem. Phys. **123**, 062201 (2005).

[8] J. P. Perdew, K. Burke, and M. Ernzerhof, Phys. Rev. Lett. **77**, 3865 (1996); **78**, 1396 (1997) (E).

[9] J. P. Perdew, V. N. Staroverov, J. Tao, and G. E. Scuseria, Phys. Rev. B **78**, 052513 (2008).

[10] K. Burke, F. G. Cruz, and K.-C. Lam, J. Chem. Phys. **109**, 8161 (1998).

[11] J. Tao, V. N. Staroverov, G. E. Scuseria, and J. P. Perdew, Phys. Rev. A **77**, 012509 (2008).

[12] Z. Yan, J. P. Perdew, and S. Kurth, Phys. Rev. B **61**, 16430 (2000).

[13] F. Furche, Phys. Rev. B **64**, 195120 (2001).

[14] M. Fuchs and X. Gonze, Phys. Rev. B **65**, 235109 (2002).

[15] B. G. Janesko, T. M. Henderson, and G. E. Scuseria, J. Chem. Phys. **130**, 081105 (2009).

[16] A. D. Becke, J. Chem. Phys. **98**, 1372 (1993).

[17] A. D. Becke, J. Chem. Phys. **98**, 5648 (1993).

[18] C. Adamo and V. Barone, J. Chem. Phys. **110**, 6158 (1999).

[19] M. Ernzerhof and G. E. Scuseria, J. Chem. Phys. **110**, 5029 (1999).

[20] P. J. Stephens, F. J. Devlin, C. F. Chabalowski, and M. J. Frisch, J. Phys. Chem. **98**, 11623 (1994).

[21] C.-O. Almbladh and U. von Barth, Phys. Rev. B **31**, 3231 (1985).

[22] F. Della Sala and A. Görling, Phys. Rev. Lett. **89**, 033003 (2002).

[23] H. Iikura, T. Tsuneda, T. Yanai, and K. Hirao, J. Chem. Phys. **115**, 3540 (2001).

[24] H. Sekino, Y. Maeda, and M. Kamiya, Mol. Phys. **103**, 2183 (2005).

[25] Y. Tawada, T. Tsuneda, S. Yanagisawa, T. Yanai, and K. Hirao, J. Chem. Phys. **120**, 8425 (2004).

[26] H. J. Monkhorst, Phys. Rev. B **20**, 1504 (1979).

[27] J. Delhalle and J.-L. Calais, Phys. Rev. B **35**, 9460 (1987).

[28] J. Heyd, G. E. Scuseria, and M. Ernzerhof, J. Chem. Phys. **118**, 8207 (2003); **124**, 219906 (2006) (E).

[29] J. P. Perdew, M. Ernzerhof, and K. Burke, J. Chem. Phys. **105**, 9982 (1996).

[30] A. V. Krukau, O. A. Vydrov, A. F. Izmaylov, and G. E. Scuseria, J. Chem. Phys. **125**, 224106 (2006).

[31] O. A. Vydrov and G. E. Scuseria, J. Chem. Phys. **125**, 234109 (2006).

[32] I. C. Gerber and J. G. Ángyán, Chem. Phys. Lett. **415**, 100 (2005).

[33] M. Kamiya, H. Sekino, T. Tsuneda, and K. Hirao, J. Chem. Phys. **122**, 234111 (2005).

[34] M. Kamiya, T. Tsuneda, and K. Hirao, J. Chem. Phys. **117**, 6010 (2002).

[35] T. M. Henderson, A. F. Izmaylov, G. E. Scuseria, and A. Savin, J. Chem. Phys. **127**, 221103 (2007).

[36] T. M. Henderson, A. F. Izmaylov, G. E. Scuseria, and A. Savin, J. Chem. Theory Comput. **4**, 1254 (2008).

[37] J. Jaramillo, G. E. Scuseria, and M. Ernzerhof, J. Chem. Phys. **118**, 1068 (2003).

[38] H. Bahmann, A. Rodenberg, A. V. Arbuznikov, and M. Kaupp, J. Chem. Phys. **126**, 011103 (2007).

[39] A. V. Arbuznikov and M. Kaupp, Chem. Phys. Lett. **440**, 160 (2007).

[40] M. Kaupp, H. Bahmann, and A. V. Arbuznikov, J. Chem. Phys. **127**, 194102 (2007).

[41] D. M. Bylander and L. Kleinman, Phys. Rev. B **41**, 7868 (1990).

[42] A. Savin and H.-J. Flad, Int. J. Quantum Chem. **56**, 327 (1995).

[43] E. Livshits and R. Baer, Phys. Chem. Chem. Phys. **9**, 2932 (2007).

[44] E. Livshits and R. Baer, J. Phys. Chem. A **112**, 12789 (2008).

[45] I. C. Gerber and J. G. Ángyan, Chem. Phys. Lett. **415**, 100 (2005).

[46] O. A. Vydrov, J. Heyd, A. V. Krukau, and G. E. Scuseria, J. Chem. Phys. **125**, 074106 (2006).

[47] J. Toulouse, F. Colonna, and A. Savin, J. Chem. Phys. **122**, 014110 (2005).

[48] R. Pollet, F. Colonna, T. Leininger, H. Stoll, H.-J. Werner, and A. Savin, Int. J. Quantum Chem. **91**, 84 (2003).

[49] A. Savin, in *Recent Developments and Applications of Modern Density Functional Theory* (Elsevier, B. V., 1996).

[50] P. M. W. Gill, R. D. Adamson, and J. A. Pople, Mol. Phys. **88**, 1005 (1996).

[51] P. M. W. Gill and R. D. Adamson, Chem. Phys. Lett. **261**, 105 (1996).

[52] D. L. Strout and G. E. Scuseria, J. Chem. Phys. **102**, 8448 (1995).

[53] M. C. Strain, G. E. Scuseria, and M. J. Frisch, Science **271**, 51 (1996).

[54] F. Della Sala and A. Görling, J. Chem. Phys. **115**, 5718 (2001).

[55] J. Jaramillo, M. Ernzerhof, and G. E. Scuseria, J. Chem. Phys. **118**, 1068 (2003).

[56] L. M. Constantin, J. P. Perdew, and J. Tao, Phys. Rev. B **73**, 205104 (2006).

[57] J. Heyd and G. E. Scuseria, J. Chem. Phys. **120**, 7274 (2004).

[58] T. M. Henderson, B. G. Janesko, and G. E. Scuseria, J. Chem. Phys. **128**, 194105 (2008).

[59] Gaussian Development Version, Revision D.01, M. J. Frisch, G. W. Trucks, H. B. Schlegel, G. E. Scuseria, M. A. Robb, J. R. Cheeseman, J. A. Montgomery, Jr., T. Vreven, G. Scalmani, B. Mennucci, V. Barone, G. A. Petersson, M. Caricato, H. Nakatsuji, M. Hada, M. Ehara, K. Toyota, R. Fukuda, J. Hasegawa, M. Ishida, T. Nakajima, Y. Honda, O. Kitao, H. Nakai, X. Li, H. P. Hratchian, J. E. Peralta, A. F. Izmaylov, K. N. Kudin, J. J. Heyd, E. Brothers, V. N. Staroverov, G. Zheng, R. Kobayashi, J. Normand, J. L. Sonnenberg, F. Ogliaro, M. Bearpark, P. V. Parandekar, G. A. Ferguson, N. J. Mayhall, S. S. Iyengar, J. Tomasi, M. Cossi, N. Rega, J. C. Burant, J. M. Millam, M. Klene, J. E. Knox, J. B. Cross, V. Bakken, C. Adamo, J. Jaramillo, R. Gomperts, R. E. Stratmann, O. Yazyev, A. J. Austin, R. Cammi, C. Pomelli, J. W. Ochterski, P. Y. Ayala, K. Morokuma, G. A. Voth, P. Salvador, J. J. Dannenberg, V. G. Zakrzewski, S. Dapprich, A. D. Daniels, M. C. Strain, O. Farkas, D. K. Malick, A. D. Rabuck, K. Raghavachari, J. B. Foresman, J. V. Ortiz, Q. Cui, A. G. Baboul, S. Clifford, J. Cioslowski, B. B. Stefanov, G. Liu, A. Liashenko, P. Piskorz, I. Komaromi, R. L. Martin, D. J. Fox, T. Keith, M. A. Al-Laham, C. Y. Peng, A. Nanayakkara, M. Challacombe, W. Chen, M. W. Wong, and J. A. Pople, Gaussian, Inc., Wallingford CT, 2007.

[60] J. P. Perdew and Y. Wang, Phys. Rev. B **45**, 13244 (1992).

[61] B. J. Lynch and D. G. Truhlar, J. Phys. Chem. **107**, 8996 (2003); **108**, 1460(E) (2004).

[62] L. A. Curtiss, K. Raghavachari, P. C. Redfern, and J. A. Pople, J. Chem. Phys. **112**, 7374 (2000).

[63] S. J. Chakravorty, S. R. Gwaltney, E. R. Davidson, F. A. Parpia, and C. F. Fischer, Phys. Rev. A **47**, 3649 (1993).

[64] G. Sperber, Int. J. Quant. Chem **5**, 189 (1971).

[65] M. Kohout, A. Savin, and H. Preuss, J. Chem. Phys. **95**, 1928 (1991).

[66] M. Levy, J. P. Perdew, and V. Sahni, Phys. Rev. A **30**, 2745 (1984) and references therein.

[67] F. E. Jorge, E. V. R. de Castro, and A. B. F. da Silva, Chem. Phys. **216**, 317 (1997).

[68] L. A. Curtiss, K. Raghavachari, P. C. Redfern, and J. A. Pople, J. Chem. Phys. **106**, 1063 (1997).

[69] V. N. Statoverov, G. E. Scuseria, J. Tao, and J. P. Perdew, J. Chem. Phys. **119**, 12129 (2003); **121**, 11507 (2004) (E).

[70] Y. Zhao, B. J. Lynch, and D. G. Truhlar, J. Phys. Chem. A **108**, 2715 (2004).

[71] Y. Zhao, N. Gónzales-García, and D. G. Truhlar, J. Phys. Chem. A **109**, 2012 (2005), **110**, 4942 (2006)(E).

[72] M. Ernzerhof and J. P. Perdew, J. Chem. Phys. **109**, 3313 (1998).

[73] J. Toulouse, A. Savin, and H.-J. Flad, Int. J. Quant. Chem. **100**, 1047 (2004).

[74] H. Bahmann and M. Ernzerhof, J. Chem. Phys. **128**, 234104 (2008).

[75] B. G. Janesko and G. E. Scuseria, J. Chem. Phys. **127**, 164117 (2007).

[76] B. G. Janesko and G. E. Scuseria, J. Chem. Phys. **128**, 084111 (2008).

[77] J. D. Talman and W. F. Shadwick, Phys. Rev. A **14**, 36 (1976).

[78] J. B. Krieger, Y. Li, and G. J. Iafrate, Phys. Rev. A **45**, 101 (1992).

[79] S. Ivanov, S. Hirata, and R. J. Bartlett, Phys. Rev. Lett. **83**, 5455 (1999).

[80] A. Görling, Phys. Rev. Lett. **83**, 5459 (1999).

[81] W. Yang and Q. Wu, Phys. Rev. Lett. **89**, 143002 (2002).

[82] J. B. Krieger, Y. Li, and G. J. Iafrate, Phys. Rev. A **46**, 5453 (1992).

[83] O. V. Gritsenko and E. J. Baerends, Phys. Rev. A **64**, 042506 (2001).

[84] A. V. Arbuznikov and M. Kaupp, Chem. Phys. Lett. **386**, 8 (2004).

[85] W. Hieringer, F. Della Sala, and A. Görling, Chem. Phys. Lett. **383**, 115 (2004).

[86] A. M. Teale and D. J. Tozer, Chem. Phys. Lett. **383**, 109 (2004).

[87] V. N. Staroverov, G. E. Scuseria, and E. R. Davidson, J. Chem. Phys. **124**, 141103 (2006).

[88] V. N. Staroverov, G. E. Scuseria, and E. R. Davidson, J. Chem. Phys. **125**, 081104 (2006).

[89] A. F. Izmalyov, V. N. Staroverov, G. E. Scuseria, E. R. Davidson, G. Stoltz, and E. Cancés, J. Chem. Phys. **126**, 084107 (2007).

[90] A. F. Izmalyov, V. N. Staroverov, G. E. Scuseria, and E. R. Davidson, J. Chem. Phys. **127**, 084113 (2007).

[91] A. Seidl, A. Görling, P. Vogl, J. A. Majewski, and M. Levy, Phys. Rev. B **53**, 3764 (1996).

[92] R. Neumann, R. H. Nobes, and N. C. Handy, Mol. Phys. **87**, 1 (1996).

[93] M. Grüning, A. Marini, and A. Rubio, Phys. Rev. B **74**, 161103(R) (2006).

[94] J. Heyd and G. E. Scuseria, J. Chem. Phys. **121**, 1187 (2004).

[95] J. Heyd, J. E. Peralta, G. E. Scuseria, and R. L. Martin, J. Chem. Phys. **123**, 174101 (2005).

[96] A. V. Arbuznikov, M. Kaupp, and H. Bahmann, J. Chem. Phys. **124**, 204102 (2006).

[97] A. V. Arbuznikov and M. Kaupp, Chem. Phys. Lett. **442**, 496 (2007).

[98] A. V. Arbuznikov and M. Kaupp, J. Chem. Phys. **128**, 214107 (2008).

[99] J. A. Pople, P. M. W. Gill, and B. G. Johnson, Chem. Phys. Lett. **199**, 557 (1992).

[100] K. Kobayashi, N. Kurita, H. Kumahora, and K. Tago, Phys. Rev. A **43**, 5810 (1993).

[101] GAUSSIAN Development Version, Revision G.01, M. J. Frisch, G. W. Trucks, H. B. Schlegel, G. E. Scuseria *et al.*, Gaussian, Inc., Pittsburgh PA, 2003.

[102] T. H. Dunning Jr., J. Chem. Phys. **90**, 1007 (1989).

[103] A. D. Becke, Phys. Rev. A **38**, 3098 (1988).

[104] J. P. Perdew, J. A. Chevary, S. H. Vosko, K. A. Jackson, M. R. Pederson, D. J. Singh, and C. Fiolhais, Phys. Rev. B **46**, 6671 (1992).

[105] S. H. Vosko, L. Wilk, and M. Nusair, Can. J. Phys. **58**, 1200 (1980).

[106] B. J. Lynch and D. G. Truhlar, J. Phys. Chem. A **107**, 8996 (2003), **108**, 1460 (2004).

[107] J. A. Pople, M. Head-Gordon, J. Fox, K. Raghavachari, and L. A. Curtiss, J. Chem. Phys. **90**, 5622 (1989).

[108] L. A. Curtiss, C. Jones, G. W. Trucks, K. Raghavachari, and J. A. Pople, J. Chem. Phys. **93**, 2537 (1990).

[109] L. A. Curtiss, P. C. Redfern, K. Raghavachari, and J. A. Pople, J. Chem. Phys. **109**, 42 (1998).

[110] COF_2 was included in the G3/99 set following Ref. [69].

[111] We perform local hybrid geometry optimizations by numerically differentiating the self-consistent GKS total energy. Analytic energy gradients for local hybrids require nonstandard terms arising from the nonlocal exchange operator. These will be straightforward to implement, and will be reported in future work.

[112] L. A. Curtiss, P. C. Redfern, K. Raghavachari, and J. A. Pople, J. Chem. Phys. **114**, 108 (2001).

[113] O. A. Vydrov and G. E. Scuseria, J. Chem. Phys. **125**, 234109 (2006).

[114] S. Ivanov and M. Levy, J. Chem. Phys. **119**, 7087 (2003).

[115] G. E. Scuseria and H. F. Schaefer, Chem. Phys. Lett. **146**, 23 (1988).

[116] M. Levy and J. Perdew, Phys. Rev. A **32**, 2010 (1985).

[117] M. Levy, Phys. Rev. A **43**, 4637 (1991).

[118] J. P. Perdew, A. Ruzsinszky, G. Csonka, O. A. Vydrov, G. E. Scuseria, V. N. Staroverov and J. Tao, Phys. Rev. A **76**, 040501 (R) (2007).

[119] J. Toulouse, P. Gori-Giorgi, and A. Savin, Int. J. Quantum Chem. **106**, 2026 (2006).

[120] A. Szabo and N. S. Ostlund, *Modern Quantum Chemistry*, 1st revised ed. (McGraw-Hill, New York, 1989).